

# SCREENING EFFECTS ON THE ELASTIC NUCLEON-NUCLEON CROSS SECTION IN RELATIVISTIC NUCLEAR MATTER

Joaquin DIAZ-ALONSO and Lysiane MORNAS  
*D.A.R.C., Observatoire de Paris-Meudon, UPR 176 CNRS  
F-92195 Meudon, France*

## ABSTRACT

We investigate the screening effects on the nucleon-nucleon elastic cross section inside nuclear matter at zero and finite temperature. The N-N interaction is described phenomenologically via meson exchanges ( $\sigma$ ,  $\pi$  and  $\omega$ ) in the framework of a relativistic lagrangian model. The expressions for the in-medium meson propagators, which take into account the effects of matter polarization and renormalized vacuum polarization, are used in the calculation of the various meson contributions to the total cross section in the one-boson exchange approximation. The final expressions allow a satisfactory fit of the Coulomb subtracted proton-proton cross section data in vacuum. At finite density or temperature the cross section is reduced as compared to the vacuum values and compatible with the existing experimental constraints. At high density the  $p$ - $p$  differential cross section gets increasingly forward and backward peaked. The  $\sigma$ - $\omega$  mixing plays a key role in the understanding of the results.

## (1) INTRODUCTION

In plasma physics the screening effects of the medium modify the effective interparticle interactions which often become very different than in vacuum. The knowledge of the effective interaction is necessary for a proper analysis of the collective behavior of the plasma. In the particular example of nuclear matter, the screening of the medium on the N-N interaction (described in vacuum by a two-nucleon potential which has a Yukawa-like expression), leads to a new form of the effective potential which is long-ranged and oscillatory [1, 2]. Such "Friedel-like" oscillations can induce, under particular conditions, the appearance of some new observable properties in the nuclear plasma, which should be the analogues of the ones encountered in degenerate electromagnetic plasmas.

Another important parameter related to the nuclear interaction, which can be modified by the screening, is the N-N cross section. It is a basic ingredient in the dynamical analysis of heavy ion collisions. Most of the early calculations in this field have been performed using a constant value of the cross section ( $\sigma = 40$  mb) or a fit of the experimental data in vacuum [3]. However, there is an ever growing bulk of evidence that the modifications introduced by in-medium effects on the cross section have a non-negligible influence on the findings of these calculations. For example, a criterion which is often used to determine the stiffness of the equation of state is the amount of transverse flow. But the collective flow, and its disappearance at the balance energy, is also used to set constraints on the magnitude of the N-N cross section in the medium. It is therefore not possible to disentangle completely the effects coming from the equation of state or from a reduced cross section. It has lately been found by several authors, from BUU [4, 5, 6, 7, 8] as well as QMD [9] or AMD [10] calculations, that a lower cross section in the medium is favoured by a detailed analysis of the transverse flow. Moreover, the cross section is an essential parameter in the calculation of transport coefficients and the knowledge of its screened behavior allows the determination of these coefficients as functions of the thermodynamical state.

There exists several calculations [11] - [19] of the in-medium elastic N-N cross section. Only one of these calculations considers finite temperature [17] as well as density. Most of them were done in the Brueckner formalism and are appropriate for the low energy range  $E_{lab} \simeq [50 - 300]$  MeV. Nevertheless, the relativistic effects should become important not only for higher energies, but (due to the medium effects) for high densities and temperatures. The purpose of this paper is to perform a fully relativistic calculation of the screening effects of the medium on the elastic N-N cross section in nuclear matter at finite density and temperature.

An acceptable (phenomenological) description of the nuclear interaction in terms of meson exchanges requires the analysis of several (scalar, pseudoscalar, vector, pseudovector and tensor) meson couplings [20]. This work is a step in a program of analysis of the screening effects on the complete nuclear interaction in nuclear matter, where all these couplings will be considered. Here we treat only the case of the exchange of scalar ( $\sigma$ ), pseudoscalar ( $\pi$ ) and vector ( $\omega$ ) meson couplings. Although the present treatment of the interaction is not complete, it allows for a good fit of the experimental data of the elastic N-N cross section <sup>1</sup> in vacuum and gives a satisfactory description of the screening effects on this parameter. Indeed, preliminary calculations including the Yukawa and derivative tensor couplings to the  $\rho$  meson, which will be published elsewhere,

---

<sup>1</sup> Here, we restrict to the Coulomb subtracted proton-proton p-p or neutron-neutron n-n cross section

indicate that the corrections to the present calculations introduced by these supplementary couplings are small. Nevertheless, due to the isospin asymmetry associated to the  $\rho$ -N coupling, the proton-neutron (p-n) elastic cross section is more affected by the  $\rho$ -exchange contributions than the p-p and n-n ones.

At highly relativistic energies, the  $\Delta(1232)$  resonance and eventually more massive resonances such as  $N^*(1440)$  are expected to play an important role. We calculated here the elastic channel of the N-N cross section and did not consider these resonances. The way in which the taking into consideration of the  $\Delta$  resonance might modify our analysis will be discussed in the last section. Basically two types of corrections will have to be considered:

First, the inelastic channels  $N + N \rightarrow N + \Delta$  and  $N + N \rightarrow \Delta + \Delta$  open at  $T_{lab} \geq 350$  MeV. At energies higher than 800 MeV, the inelastic contribution represents 50% of the total N-N cross section. The  $\Delta$  production and absorption *via* the inverse processes  $N + \Delta \rightarrow N + N$  ... *etc* mechanism is the input for the calculation of the subsequent pion production through  $\Delta$  decay ( $\Delta \rightarrow N + \pi$ ). The theoretical pion distribution and spectra obtained in this way serve as a basis for comparison with the values observed experimentally in relativistic heavy ion collisions. This important topic deserves a separate study and will be treated elsewhere.

Secondly, the  $\Delta$ 's can also appear in internal loops. They will thus modify the screening of the interaction. There exists an abundant literature on the modification of the  $\pi$  dispersion relation by the  $\Delta$  (see *e.g.* [21, 22, 23] ). This topic is not yet completely settled, especially concerning the relativistic treatment. We argue that the screening of the pion will not play an important role for the proton-proton cross section calculated here, and will discuss the case of the modifications to the  $\sigma$  and  $\omega$  dispersion relations in the last section (see section (6)). As far as we know, the modification of other mesons than the  $\pi$  by delta-hole loops has not yet been considered in the literature; this will be the subject of future work.

In section (2) we give the lagrangian model, define the Hartree equilibrium and introduce the in-medium meson propagators at finite temperature, obtained in the one-loop approximation and including the vacuum polarization effects. Section (3) is devoted to the calculation of the elastic N-N cross sections from the screened propagators in the one-boson exchange approximation. In section (4) we determine the model parameters in order to fit the available experimental data on cross section in vacuum. In section (5) we present the results with the analysis of the effects of density and temperature on this variable, and conclude in section (6) with a discussion on the possible extensions of the model.

## (2) THE MODEL AND THE MESON DISPERSION RELATIONS

### 2.1 Lagrangian density

The cross section will be calculated by considering that the nucleons are interacting through the exchange of  $\sigma$ ,  $\omega$  and  $\pi$  mesons. The dynamics of the model is given by the Lagrangian density

$$\hat{L} = \frac{i}{2} [\hat{\bar{\psi}} \gamma \cdot (\partial \hat{\psi}) - (\partial \hat{\bar{\psi}}) \cdot \gamma \hat{\psi}] - m \hat{\bar{\psi}} \hat{\psi}$$

$$\begin{aligned}
& + \frac{1}{2} [(\partial^\nu \hat{\sigma})(\partial_\nu \hat{\sigma}) - \mu_\sigma^2 \hat{\sigma}^2] \\
& + \frac{1}{2} [(\partial^\nu \hat{\pi})(\partial_\nu \hat{\pi}) - \mu_\pi^2 \hat{\pi}^2] \\
& - \frac{1}{4} \hat{F}_\omega^{\mu\nu} \hat{F}_{\omega\mu\nu} - \frac{1}{2} \mu_\omega^2 \hat{\omega}^\nu \hat{\omega}_\nu \\
& + g_\sigma \hat{\psi} \hat{\sigma} \hat{\psi} + g_\omega \hat{\psi} \gamma^\mu \hat{\omega}_\mu \hat{\psi} + g_\pi \hat{\psi} \gamma^5 \vec{\tau} \hat{\pi} \hat{\psi}
\end{aligned} \tag{1}$$

where

$$\hat{F}_\omega^{\mu\nu} = \partial^\mu \hat{\omega}^\nu - \partial^\nu \hat{\omega}^\mu \tag{2}$$

and the hat symbol over characters denotes quantum operators.

A meson-meson interaction term of the form  $\sigma \cdot \vec{\pi}^2$  is usually added to this lagrangian model in order to improve the fit of the pion-nucleon scattering amplitudes in vacuum. If the value of the associated coupling constant is properly constrained, cancellations of large contributions to the s-wave scattering lengths occur and the predictions of the model become reasonable in vacuum [24]. Nevertheless, no such cancellations occur at finite density and temperature, unless this coupling constant be differently constrained in every thermodynamical state. Moreover, for some values of the coupling strength this term can lead to difficulties related to the tachyonic poles introduced in the pion propagator by the imaginary character of the effective mass of the quasi-pion in the Hartree approximation. Finally, as we have tested, this term has no important quantitative incidence on the calculated cross sections in this approximation. Consequently, we shall not consider this interaction here.

In the calculations performed in this paper, the numerical values of the constants appearing in the Lagrangian (1) are fixed as follows: The meson and fermion masses are fixed to their "physical" values  $\mu_\sigma = 550$  MeV,  $\mu_\omega = 783$  MeV,  $\mu_\pi = 138$  MeV and  $m = 939$  MeV. The solution of the model in the relativistic Hartree approximation (first order approximation in our scheme) leads to the equation of state of the plasma [25]. Then, we chose for the  $\omega$  and  $\sigma$  coupling constants the values which give a satisfactory fit of the saturation properties in this approximation. These are  $g_\sigma^2 = 183.3 (\mu_\sigma/m)^2$  and  $g_\omega^2 = 114.7 (\mu_\omega/m)^2$ . With these values, saturation is attained at  $P_{f0} = 1.40 fm^{-1}$  with a binding energy  $E_b = -15.85$  MeV. Nevertheless, in the higher order approximations leading to the calculation of the in-medium elastic cross sections we shall often use different values of the coupling constants in order to fit the experimental values of this parameter in the vacuum (see section 4). This is justified because in our cluster expansion scheme [26] the values of the parameters must be redefined at every order.

## 2.1 Dispersion relations

Beyond the Hartree approximation, we treat the in-medium N-N interaction as mediated by dressed mesons. The one-loop  $\omega - \sigma$  meson propagators at  $T = 0$  have been obtained for the first time in Ref. [27]. The dispersion relations and propagators of the mesons at finite temperature used here were obtained from a linear kinetic analysis of perturbations around the

Hartree ground state, starting from the relativistic quantum B.B.G.K.Y. hierarchy [28, 29]. This cluster expansion differs from the usual loop expansion, but one can show that the first order of the B.B.G.K.Y. expansion coincides, at zero temperature, with the one-loop approximation [2]. Nevertheless, the higher order corrections in the kinetic expansion differ from the results of many-loop calculations.

Renormalized vacuum polarization contributions are crucial in obtaining a physically reasonable behavior of the propagation modes [29]. A first analysis of the structure of the one-loop  $\sigma - \omega$  propagators at zero temperature has been performed by Lim and Horowitz [30] in the semiclassical approximation (no vacuum polarization effects). It has been partially extended to the finite temperature case with vacuum effects in [31] and (completed with a study of the the zero-sound modes and a improved choice of the renormalization point) in Ref. [32].

The dispersion relation matrix as obtained in Ref. [29] has the form

$$D(k) = \begin{bmatrix} -k^\mu k^\nu + (k^2 - \mu_\omega^2) g^{\mu\nu} & g_\sigma g_\omega \Pi_{\sigma\omega}^\mu(k) & 0 \\ -g_\omega^2 \Pi_\omega^{\mu\nu}(k) & & \\ -g_\sigma g_\omega \Pi_{\sigma\omega}^\nu(k) & -k^2 + \mu_\sigma^2 - g_\sigma^2 \Pi_\sigma(k) & 0 \\ 0 & 0 & k^2 - \mu_\pi^2 + g_\pi^2 \Pi_\pi(k) \end{bmatrix} \quad (3)$$

where the general expressions for the polarizations  $\Pi(k)$  of the meson fields as functions of the thermodynamical state (density and temperature) and 4-momentum  $k^\mu = (\omega, \vec{q})$  are summarized in appendix A. The  $\pi$  propagation is decoupled from the dynamics of the other mesons because of parity conservation. There is a mixing between the  $\sigma$  and longitudinal- $\omega$  propagation modes. The dynamics of the mesons in the medium is affected by the real as well as the imaginary parts of the polarizations. As mentioned above, the analysis of the propagation modes associated to the real components of the polarizations has been performed already. Let us make some comments about the behavior of the imaginary polarizations (see also appendix A.2):

a) Except for the mixing terms, the baryon and antibaryon contributions to the imaginary parts of the polarizations have opposite signs. The antibaryon contributions vanish in the  $T = 0$  limit and the baryon contributions reduce to the usual expression for the matter contribution to the imaginary polarizations. The vacuum contributions to the imaginary parts have the same form as in the  $T = 0$  case and are finite.

b) For time-like modes, there are two regions in the first sector of the  $q - \omega$  plane separated by the parabola defined by

$$\omega = \sqrt{q^2 + 4M^2} \quad (\Delta = 1 - 4M^2/(\omega^2 - q^2) = 0). \quad (4)$$

Here,  $M = m - g_\sigma \langle \sigma \rangle$  is the effective baryon mass. As in the  $T = 0$  case the imaginary parts vanish in the region between this parabola and the diagonal  $\omega = q$  ( $\Delta < 0$ ), and the

modes are undamped there. Over this parabola ( $\Delta > 0$ ) the modes are damped by the decay into particle-antiparticle pairs.

c) For spacelike modes in the  $T = 0$  limit, the imaginary parts vanish outside the region defined by

$$\sqrt{(p_F - q)^2 + M^2} - \sqrt{p_F^2 + M^2} < \omega < \sqrt{(p_F + q)^2 + M^2} - \sqrt{p_F^2 + M^2} \quad (5)$$

( $p_F$  is the Fermi momentum) where the modes are damped by the decay into particle-hole pairs. This region arises because, at  $T = 0$ , the baryonic Fermi factor in Eq.(57) becomes a step function. At finite temperature the imaginary parts are finite for any space-like mode. Nevertheless, for moderate temperatures, the behavior of the Fermi factors makes the imaginary parts small outside the particle-hole region.

### (3) THE O.B.E. CROSS SECTION

The in-medium cross section is calculated by describing the nucleon interaction through the exchange of single dressed  $\sigma$ ,  $\omega$  and  $\pi$  mesons. The generic O.B.E. diagram is given in Fig.(1). The fermion lines correspond to the nucleons in the medium which acquire an effective mass and momentum from the ambient mean field in thermodynamic equilibrium. The properties of the effective nucleons are calculated in the Hartree approximation with renormalized vacuum fluctuations taken into account [33]. The dressed propagator matrix of the mesons is obtained by the inversion of the dispersion relation matrix (3).

#### 3.1 Dressed meson propagators

The expressions of the polarizations given in appendix A were calculated, without loss of generality, in a frame (R1) where the background fluid is at rest and the momentum transfer is  $k^\mu = (\omega, 0, 0, q)$ . In the following we will be working in the center of mass system of the collision (R2) in which the matter comoving system travels with the quadrivelocity  $u^\mu$ . It will therefore be more convenient to put the dispersion relations and propagators under a compact covariant form.

We define the auxiliary quadrivector  $\eta^\mu$  and the projectors onto the longitudinal ( $\Lambda^{\mu\nu}$ ) and transverse ( $\mathcal{T}^{\mu\nu}$ ) modes as follows:

$$\eta^\mu = u^\mu - \frac{k \cdot u}{k^2} k^\mu \quad (6)$$

$$\tilde{g}^{\mu\nu} = g^{\mu\nu} - \frac{k^\mu k^\nu}{k^2} \quad (7)$$

$$\mathcal{T}^{\mu\nu} = \tilde{g}^{\mu\nu} - \frac{\eta^\mu \eta^\nu}{\eta^2} \quad (8)$$

$$\Lambda^{\mu\nu} = \frac{\eta^\mu \eta^\nu}{\eta^2} \quad (9)$$

so that the polarizations now read

$$\Pi_{\sigma\omega}^\mu = \Pi_\times \eta^\mu / [\eta^2]^{1/2} \quad (10)$$

$$\Pi_\omega^{\mu\nu} = -\Pi_{\omega L} \Lambda^{\mu\nu} - \Pi_{\omega T} \mathcal{T}^{\mu\nu} \quad (11)$$

in terms of the longitudinal, transverse and mixing parts  $\Pi_{\omega L}$ ,  $\Pi_{\omega T}$  and  $\Pi_\times$ . These scalar quantities are related to the components  $\Pi_\omega^{00}$ ,  $\Pi_\omega^{11}$ ,  $\Pi_{\sigma\omega}^0$  defined in appendix A by

$$\Pi_{\omega L} = \frac{\omega^2 - q^2}{q^2} \Pi_\omega^{00} \quad ; \quad \Pi_{\omega T} = \Pi_\omega^{11} \quad ; \quad \Pi_\times^2 = \frac{q^2 - \omega^2}{q^2} (\Pi_{\sigma\omega}^0)^2$$

The expression for meson propagator matrix becomes

$$G^{mn} = \begin{pmatrix} G_\omega^{\mu\nu} & G_{\sigma\omega}^\mu & 0 \\ G_{\omega\sigma}^\mu & G_\sigma & 0 \\ 0 & 0 & G_\pi \end{pmatrix} \quad (12)$$

where the different elements (propagators) are given by

$$G_\sigma = i \frac{k^2 - \mu_\omega^2 + g_\omega^2 \Pi_{\omega L}}{(k^2 - \mu_\sigma^2 + g_\sigma^2 \Pi_\sigma)(k^2 - \mu_\omega^2 + g_\omega^2 \Pi_{\omega L}) + g_\sigma g_\omega \Pi_\times^2} \quad (13)$$

$$G_\omega^{\mu\nu} = -i \left[ \mathcal{T}^{\mu\nu} \frac{1}{k^2 - \mu_\omega^2 + g_\omega^2 \Pi_{\omega T}} - \frac{k^\mu k^\nu}{\mu_\omega^2 k^2} + \Lambda^{\mu\nu} \frac{k^2 - \mu_\sigma^2 + g_\sigma^2 \Pi_\sigma}{(k^2 - \mu_\sigma^2 + g_\sigma^2 \Pi_\sigma)(k^2 - \mu_\omega^2 + g_\omega^2 \Pi_{\omega L}) + g_\sigma g_\omega \Pi_\times^2} \right] \quad (14)$$

$$= -i \left[ G_{\omega T} \mathcal{T}^{\mu\nu} + G_{\omega L} \Lambda^{\mu\nu} - \frac{k^\mu k^\nu}{\mu_\omega^2 k^2} \right] \quad (15)$$

$$G_{\sigma\omega}^\mu = -i \eta^\mu \frac{g_\sigma g_\omega \Pi_\times}{(k^2 - \mu_\sigma^2 + g_\sigma^2 \Pi_\sigma)(k^2 - \mu_\omega^2 + g_\omega^2 \Pi_{\omega L}) + g_\sigma g_\omega \Pi_\times^2} \quad (16)$$

$$= -i \eta^\mu G_\times$$

$$G_\pi = i \frac{1}{k^2 - \mu_\pi^2 + g_\pi^2 \Pi_\pi} \quad (17)$$

In inverting the dispersion matrix Eq.(3), the meson branches associated to the zeroes of the determinant become poles of the meson propagators. We are interested here in the spacelike region of the  $q - \omega$  plane and, when vacuum polarization is taken into account, there are only three poles of the propagator in this region, associated to the "tachyonic" branches of the mixed  $\sigma$ -longitudinal, transverse and pion modes [29]. These branches come from the vacuum

polarization terms and arise at large  $k$ , where the one-loop calculations fails [34]. In fact, for these values of  $k$  (short distances) the point particle approach becomes inadequate and the structural properties of nucleons must be taken into account. In a more fundamental theory of pointlike particles, vertex corrections could be calculated self-consistently (see *e.g.* [35]). In nuclear matter models, such corrections have been introduced in analogy with the QED case, with the suppression of high momentum transfer arising from the virtual Bremsstrahlung of neutral vector  $\omega$  mesons [36, 37]. In our phenomenological model, this can as well be done through the introduction of phenomenological monopolar form factors for the nucleon at every vertex in the boson exchange diagrams as well as at every vertex in the loop calculation of the boson propagators. This leads to new expressions which, in  $k$ -space, are obtained from the original ones by multiplying every coupling constant by the corresponding form factor. These form factors have the generic form

$$\mathcal{F}(k) = (\Lambda^2 - \mu^2)/(\Lambda^2 - k^2) \quad (18)$$

where  $\mu$  is the scalar, vector or pion meson mass in every case and  $\Lambda$  is a cut-off parameter. After the introduction of the form factors, if the cut-offs are in appropriate ranges, the spurious "tachyonic branches" as well as the associated poles of the meson propagators on the  $\omega < q$  region disappear. The renormalized vacuum contributions are crucial in obtaining physical (stable and causal) propagation modes [29]. If they are neglected, new unphysical spacelike modes are present at small  $q$  which can not be eliminated by the form factors and adulterate the pole structure of the propagators.

### 3.2 Transition matrix and N-N cross section

The O.B.E. amplitude  $\mathcal{M}$  is obtained in the first Born approximation from the diagram of Fig.(1). In condensed form, we have

$$\mathcal{M} = \sum_{m,n=\sigma,\omega,\pi} (\bar{U}_3 \Gamma_m U_1) G_{31}^{mn} (\bar{U}_4 \Gamma_n U_2) - \text{exchange} \quad (19)$$

In this expression the  $U$ 's are the spinors defining the incoming ( $U_1, U_2$ ) and outgoing ( $U_3, U_4$ ) nucleon states. The indices  $i = 1, 2, 3, 4$  stand for the effective momenta  $(p_i^\mu)^* = p_i^\mu - g_\omega < \omega^\mu >$  and the spin-isospin quantum numbers  $s_i, t_i$ .  $G_{31}^{mn}$  is the propagator matrix (12) which depends on the momentum transfer  $k_{31}^\mu = p_1^{\mu*} - p_3^{\mu*}$ .  $\Gamma$  is the coupling matrix defined by

$$\Gamma = \begin{pmatrix} -ig_\omega \gamma^\mu \\ ig_\sigma \\ g_\pi \gamma_5 \vec{\tau} \end{pmatrix} \quad (20)$$

In the explicit calculation of the transition matrix from these formulae, all the coupling constants in  $G^{mn}$  and  $\Gamma_m$  are to be multiplied by the corresponding form factors. The exchange term is obtained by interverting the indices 3 and 4.



In the referential (R1) where the fluid is at rest,  $u^\mu = (1, \vec{0})$  and

$$p_1^\mu = P^\mu + k^\mu/2 \quad ; \quad p_2^\mu = K^\mu - k^\mu/2 \quad ; \quad p_3^\mu = P^\mu - k^\mu/2 \quad ; \quad p_4^\mu = K^\mu + k^\mu/2$$

with

$$k^\mu = (\omega, 0, 0, q)$$

In the center of mass of the collision (referential (R2)), the background fluid moves with a velocity  $u^\mu = (\gamma, \gamma\vec{v})$  parametrized by

$$\vec{v} = \begin{pmatrix} v \sin \alpha \sin \varphi \\ v \sin \alpha \cos \varphi \\ v \cos \alpha \end{pmatrix} \quad (21)$$

The momenta of the incident and scattered particles are (energy conservation is already taken into account)

$$p_1^\mu = (E, \vec{p}) \quad , \quad p_2^\mu = (E, -\vec{p}) \quad , \quad p_3^\mu = (E, \vec{p}') \quad , \quad p_4^\mu = (E, -\vec{p}') \quad ,$$

the scattering angle is  $\theta$  defined by  $\vec{p} \cdot \vec{p}' / \sqrt{(\vec{p}^2 \vec{p}'^2)} = \cos \theta$ . The momentum transfers for the direct ( $k_{31}$ ) and exchange ( $k_{41}$ ) diagrams are

$$\begin{aligned} k_{31}^\mu &= (0, \vec{p} - \vec{p}') \\ k_{41}^\mu &= (0, \vec{p} + \vec{p}') \end{aligned}$$

One goes from (R1) to (R2) by performing a boost of four-velocity  $(\gamma, \gamma\vec{v})$  and a rotation. In the referential (R1),

$$\begin{aligned} k_{31}^\mu(R1) &= (\omega_\ominus, \vec{q}_\ominus) \\ k_{41}^\mu(R1) &= (\omega_\oplus, \vec{q}_\oplus) \\ \omega_{(\ominus)} &= \gamma v p [\pm \sin \alpha \sin \varphi \sin \theta - \cos \alpha (1 \mp \cos \theta)] \\ q_{(\ominus)} &= [\omega_{(\ominus)}^2 + 2p^2 (1 \mp \cos \theta)]^{1/2} \end{aligned}$$

The expression of the differential cross section for elastic N-N scattering in the center of mass of the two colliding particles is given by

$$d\sigma/d\Omega = 1/(64\pi^2 s) |\mathcal{M}|^2 \quad (22)$$

where  $s$  is the Mandelstam variable  $s = 4E^2$ . In the following we consider only the spin-averaged cross section obtained by replacing  $|\mathcal{M}|^2$  by  $\overline{|\mathcal{M}|^2} = (1/4) \sum_{s_1, s_2, s_3, s_4} |\mathcal{M}|^2$  in Eq. (22). We obtain the  $p$ - $p$  cross-section for the isospin quantum numbers  $t_1 = t_2 = t_3 = t_4 = 1$  and the  $n$ - $n$

cross section for  $t_1 = t_2 = t_3 = t_4 = 0$ .  $\sigma_{pp}$  and  $\sigma_{nn}$  are equal in our approximation where the Coulomb interaction was subtracted and the neutron and proton masses taken to be equal.

The explicit formula for  $d\sigma/d\Omega$  is given in Appendix B in terms of the Mandelstam variables.

In the next section the values of the coupling constants and the cut-offs of the form factors will be fixed in order to fit the cross section experimental data in vacuum.

## (4) CHOICE OF MODEL PARAMETERS

### 4.1 Vacuum effects

We recall that the vacuum effects were renormalized (see appendix A) in such a way that the contribution of the vacuum polarizations at vanishing temperature and density cancel on the mass shell of the mesons:

$$\Pi_i^{vac}(k = k_i) = 0 \text{ at } k_i^2 = \mu_i^2, \quad i = \{\sigma, \omega, \pi\} \quad (23)$$

For other values of  $k$  however, the polarisation of the vacuum will bring a contribution to the free propagator

$$G_i^0(k) = \frac{1}{k^2 - \mu_{i*}^2(k)} \quad , \quad \mu_{i*}^2(k) = \mu_i^2 - g_i^2(k)\Pi_i^{vac}(k)$$

$$\text{with } g_i(k) = g_i \cdot \frac{\Lambda_i^2 - \mu_i^2}{\Lambda_i^2 - k^2} \quad (24)$$

The taking into account of the vacuum polarization has the effect of reducing the effective  $k$ -dependent meson masses  $\mu_{i*}(k)$  at high momentum transfer  $k$ . As mentioned above, the vacuum polarization contributions are essential in obtaining a reasonable pole structure of the propagator [29]).

### 4.2 Fitting procedure

Our model includes only  $\pi$ ,  $\sigma$ ,  $\omega$  meson exchange. It is a minimal model which allows to reproduce the general features of the nucleon-nucleon cross section with only five parameters: the couplings of the scalar and vector mesons  $g_\sigma$ ,  $g_\omega$  and the cutoffs  $\Lambda_\sigma$ ,  $\Lambda_\omega$ ,  $\Lambda_\pi$ . We fix the pion-nucleon coupling constant from experimental data on pion-nucleon scattering. Recent work (see *e.g.* [38]) quote a value slightly lower ( $g_\pi^2/(4\pi) = 13.7$ ) than the standard textbook value ( $g_\pi^2/(4\pi) = 14.4$ ). We chose the latter one in order to be consistent with previous work. This will have no important incidence on our results anyway. The meson masses are kept fixed at their physical value  $\mu_\pi = 138$  MeV and  $\mu_\omega = 783$  MeV. The scalar meson is not physical but is a phenomenological way of describing correlated two pion exchange, so that the constraint on its mass is less important <sup>2</sup>. We take the standard Bonn potential value  $\mu_\sigma = 550$  MeV. The value of the  $\omega$ - $N$ - $N$  coupling constant is not very well known experimentally. This

---

<sup>2</sup>The  $\sigma$  might be identified with the  $f_0$  (400-1200) broad resonance mentioned in the last issue of the Particle Data Book [39]. The controversy about the identification of this scalar particle as a broad  $\pi - \pi$  resonance was revived by recent observations [40]

situation may be improved by future planned experiments near the  $\omega$  production threshold. Quark models [41, 42, 43] predict  $g_\omega \simeq 8.5 - 8.8$ . From the decay width  $\Gamma(\omega \rightarrow e^+e^-)$  and in the vector dominance approximation, a value  $g_\omega \simeq 8.6$  can be estimated. On the other hand, the Bonn model value  $g_\omega^2/(4\pi) \simeq 20.$ , obtained by fitting the nucleon scattering phase shifts is much larger, but it can be reduced by taking into account correlated  $\pi - \rho$  exchange. We will let  $g_\omega$  vary and will see in the next subsection that our fit yields values in the range 8-9. The cutoffs should be chosen larger than the mass of the meson exchanged. There is also an upper limit set by the constraint that the tachyonic modes of the dispersion relations should be removed (see the discussion of section (3.1) and Ref. [29]). In practice, we restrict the search to the range  $1.5 \mu_i < \Lambda_i < 1700$  MeV.

Publication of experimental data is scattered throughout the literature. Recent compilations and smooth fitting of the available data are to be found in Refs. [44, 45]. These compilations do not subtract the Coulomb scattering in  $p$ - $p$  data at low momentum exchange. Coulomb scattering is most important at low energy  $T_{lab} < 40$  MeV and/or scattering angles  $\theta < 10^\circ - 20^\circ$ . We consider here a model of the nuclear interaction only, since the cross section we are calculating is intended for use in the current models of nuclear matter (BUU, QMD ...), where the Coulomb interaction can be neglected. Simple fits of Coulomb-subtracted experimental data are given by Cugnon *et al.* [3, 46] for use in their cascade model. Some Coulomb-subtracted data points are also given in the older paper of Chen *et al.* [47].

We performed a simultaneous fit of the total elastic cross-section *and* the differential cross section at 9 distinct values of the c.m. energy. The fit was obtained using a weighed least-squares method where the data points are chosen as follows: For the total cross section  $\sigma_{pp}$ , we used 12 points distributed over the energy range  $T_{lab} \in [40-1000]$  MeV. For the differential cross section,  $d\sigma_{pp}/d\Omega$ , we used 8 points distributed in the range of scattering angles  $\theta \in [10^\circ - 90^\circ]$  for each value of the energy  $T_{lab} = 60, 100, 250, 350, 460, 560, 660, 800, 1000$  MeV. Fitting only  $d\sigma_{pp}/d\Omega$  would in principle be enough since  $\sigma_{pp}$  is obtained by integrating over  $\theta$ , but we obtain better results by taking  $\sigma_{pp}$ -data with a weight of 10 % - 20 % into account. Very-low or very-high energy data for  $d\sigma_{pp}/d\Omega$  was also attributed a lower weight. We found in this way  $\chi^2$  values in the range 10 - 12.

Due to the reduced number of free parameters, our model is not be expected to do as accurate a job as the last Bonn [20, 48, 49], Nijmegen [50] or Argonne [51] potentials for example. Nevertheless it will be seen in the remaining that a reasonably good fit can be obtained for the  $p$ - $p$  (and, which is equivalent here,  $n$ - $n$ ) total and differential elastic cross section. It is more difficult to reproduce the  $p$ - $n$  cross sections. As a matter of fact, the  $T = 1$  isospin channel which is necessary for the calculation of  $p$ - $n$  scattering requires the presence of the  $\rho$ -meson exchange term. For this reason, in this paper we show only results for the  $p$ - $p$  cross-section. Inclusion of more mesons ( $\rho, \eta, \delta$ ) and calculation of the  $p$ - $n$  cross section is currently under way.

### 4.3 Fitting parameters

Depending on the details of the fitting procedure, we found several equivalent parameter sets. The total elastic  $p$ - $p$  cross section  $\sigma_{pp}$  is well reproduced in the energy range [40-1000] MeV by the parameter sets (A,B,C). (see Fig. 2). We also quote the somewhat extreme choices (D,E,F).

	$g_\sigma$	$g_\omega$	$\Lambda_\sigma$	$\Lambda_\omega$	$\Lambda_\pi$
set A	3.80	9.31	1298.8	1240.5	362.1
set B	3.27	8.38	1622.0	1324.7	355.2
set C	4.87	8.99	951.3	1255.3	397.4
set D	7.93	8.93	703.3	1237.3	376.1
set E	8.9	37.7	1643.2	903.2	587.2
	$m_\sigma$	$g_\omega$	$\Lambda_\sigma$	$\Lambda_\omega$	$\Lambda_\pi$
set F	763.3	8.06	912.2	1348.5	390.2

By comparing our results at finite density and temperature, this will allow to investigate the sensitivity of our conclusions to the choice of model parameters. (D) is obtained by fixing the coupling constants to their saturation values (see section (2)), so that it contains only the three cutoffs as free parameters. (F) is obtained by fixing the coupling constant of the  $\sigma$  meson equal to that of the pion and instead let vary the  $\sigma$  mass. Sets (A,B,C,D,F) all correspond to the same minimum in parameter space. Sets (D) and (F) have to pay for a too high  $g_\sigma$  by a correspondingly low  $\Lambda_\sigma$ . Set (E) corresponds to another (not very stable) minimum in parameter space. It is somewhat better at low energy but grows rapidly bad at energies higher than 500 MeV. There a very strong vector coupling is castigated by a small  $\Lambda_\omega$ . The best choice is set (A), then we have (B) > (C) > (D) > (F) > (E). In all cases we notice that the cut-off parameter of the pion is smaller than usually admitted in Bonn parametrizations. This is due to the absence of compensation by the  $\rho$  meson. Preliminary results indeed show that the inclusion of the  $\rho$  meson allows higher values of  $\Lambda_\pi$ . Still the  $\Lambda_\pi$ 's of all sets shown here are always above twice and a half the pion mass.

The differential cross section is somewhat more difficult to fit accurately (see Fig. 3). It is possible to perform a good quantitative fit at high energies. At lower energies, the fit becomes qualitative. The same remarks about the goodness (badness) of the parameter sets as for the total cross section apply here. The low energy behavior would be improved by increasing  $g_\sigma$ .

If we look at the contributions of each meson separately, we see that the value of the cross section is essentially driven by the  $\sigma$  and  $\omega$  mesons. In a way similar to what happens for the nuclear potential [29], the value of  $\sigma_{pp}$  results from a delicate balance of  $\sigma$  and  $\omega$  contributions. The pion describes the low momentum-transfer, long-range part and the detail of the differential cross section at forward angles.

## (5) RESULTS AND DISCUSSION

As a first important statement, it is found that the various choices of fitting parameters essentially give the same behavior at finite density and temperature. We display here results for the set of parameters (A), and comment about the other sets when appropriate.

### 5.1 In-medium cross section from screening

The total elastic  $p$ - $p$  cross section at zero temperature is displayed in Fig. 4 for the parameter

set (A) and for various values of the density. It is seen that it decreases with increasing density. The reduction is larger at smaller momentum transfer and energy, so that the total cross section becomes approximately constant throughout the whole energy interval for  $n \simeq n_{sat}$ . Further increasing the density does not much modify  $\sigma_{pp}$ .

We do not observe significant differences for the total  $p$ - $p$  cross section calculated with parameters sets (A,B,C,D,F). For sets (A,B,C),  $\sigma_{pp}$  ( $n \geq 2 n_{sat}$ ) settles around  $\simeq 17$  mb for all  $T_{lab}$ . For sets (D,F), we have a somewhat lower value  $\sigma_{pp}$  ( $n \geq 2 n_{sat}$ )  $\simeq 15.5$  mb, but we saw that both models had a too high scalar coupling  $g_\sigma$  and a too low scalar  $\Lambda_\sigma$  cutoff. The general features (low-density reduction, flattening to a  $T_{lab}$ -independent value, constant value at high density) are also obtained with set (E), but it settles to a higher value  $\sigma_{pp}$  ( $n \geq 2 n_{sat}$ )  $\simeq 71$  mb. This high value is to be traced to the unreasonably strong  $g_\omega$  and low cutoff  $\Lambda_\omega$ .

We also calculated the total  $p$ - $p$  cross section at finite temperature. The ratio of the value of the cross section in the medium to its value in the vacuum is shown in Fig. 5 as a function of density  $n/n_{sat}$  for seven values of the temperature  $T=0, 40, 80, 120, 160, 200$  and  $240$  MeV and for two values of the energy of the beam energy  $T_{lab} = 100$  MeV and  $T_{lab} = 300$  MeV. This same ratio is displayed as a function of temperature on Fig. 6a for five values of the density  $n/n_{sat} = 0, 0.1, 1., 2.$  and  $4.$  for the same values of the beam energy. These results are summarized in Fig. 7 as a contour plot in the density-temperature plane for incident particle energies  $T_{lab} = 100, 300, 500$  MeV.

At  $n = 0$ , a similar behavior is obtained with increasing the temperature as at  $T = 0$  with increasing density (the  $\sigma_{pp}$  cross section decreases at high  $T$ ) but the temperature dependence is not as strong as the density dependence: There is almost no difference between the  $T = 0$  and  $T = 120$  curves. The same quantitative effect is obtained by heating the vacuum at  $T = (150, 170, 200)$  MeV, or by compressing cold matter at  $n = (0.1, 0.5, 1)$  times the saturation density. The cross section at  $n = 0$  becomes flat over the energy range  $[40 - 1000]$  MeV at  $T=250$  MeV.

At fixed non vanishing temperature, the cross section is a nonmonotonous function of the density as can be seen on Fig. 5. This figure also reveals that the cross section is more sensitive to temperature in the density range of interest for nuclear collisions  $n/n_{sat} = 0.2 - 2$ .

At fixed non-vanishing density, the cross section is non monotonous as a function of the temperature. It first slightly increases, reaches a maximum and decreases rather rapidly at high  $T$ . The turnpoint temperature increases with increasing density. In brief, the behavior of the cross section  $\sigma_{pp}$  with varying  $T$  qualitatively follows that of the nucleon effective mass (compare Figs. 6a and 6b).

The remarks done on the example of parameter set (A) as to the behavior of the total cross section with temperature hold for (B,C,D,F) parameter sets as well, save some insignificant quantitative differences.

Let us finally discuss the density and temperature dependence of the differential  $p$ - $p$  cross section (see Fig. 8 and Fig 3c). Since  $d\sigma_{pp}/d\Omega$  is quantitatively not so well reproduced as the total one, we have to be more cautious in our conclusions. We nevertheless notice some general features: at high density or temperature, the differential  $p$ - $p$  cross section becomes very forward peaked (or equivalently backward peaked since the  $p$ - $p$  cross section is symmetric around  $\theta = 90^\circ$ ). This trend is not affected by the same ‘‘saturation’’ effect as for the integrated cross section.

At low density on the other hand, forward scattering is slightly suppressed with respect to the free value.

The behavior of the cross section as a function of density and temperature can directly be related to that of the polarizations. As a matter of fact, the polarizations appreciably differ from zero when the momentum transferred by the meson is lower than the threshold value  $\sqrt{-k^2} = 2 p_F$  for particle-hole production/recombination<sup>3</sup>. When this occurs, the mixing between the sigma meson and the longitudinal mode of the omega meson through particle-hole loops is important, and the balance between the attractive and repulsive parts of the interaction is disturbed.

Let us recast the propagators of the mesons inside the medium in a form as close as possible to the free one (*e.g.*  $G_\sigma^0 = 1/(k^2 - [\mu_\sigma^{\text{vac}}(k)]^2)$ ):

$$G_\sigma = \frac{K_{\text{mix}}}{k^2 - [\mu_\sigma^{\text{eff}}(k)]^2 + i\mu_\sigma^{\text{eff}}(k)\Gamma_\sigma(k)} \quad (25)$$

$$G_\omega = \frac{K_{\text{mix}}}{k^2 - [\mu_{\omega L}^{\text{eff}}(k)]^2 + i\mu_{\omega L}^{\text{eff}}(k)\Gamma_{\omega L}(k)} \Lambda^{\mu\nu} + \frac{1}{k^2 - [\mu_{\omega T}^{\text{eff}}(k)]^2 + i\mu_{\omega T}^{\text{eff}}(k)\Gamma_{\omega T}(k)} \mathcal{T}^{\mu\nu} \quad (26)$$

with

$$[\mu_\sigma^{\text{eff}}(k)]^2 = \mu_\sigma^2 - g_\sigma^2 \mathcal{R}e \Pi_\sigma(n, T, k) \quad (27)$$

$$1/\Gamma_\sigma = \mu_\sigma^{\text{eff}}/g_\sigma^2 \mathcal{I}m \Pi_\sigma(n, T, k) \quad (28)$$

(and similarly for  $\pi$ ,  $\omega L$  and  $\omega T$ ), and

$$K_{\text{mix}} = \frac{(k^2 - \mu_\omega^2 + g_\omega^2 \Pi_{\omega L})(k^2 - \mu_\sigma^2 + g_\sigma^2 \Pi_\sigma)}{(k^2 - \mu_\omega^2 + g_\omega^2 \Pi_{\omega L})(k^2 - \mu_\sigma^2 + g_\sigma^2 \Pi_\sigma) + g_\sigma g_\omega \Pi_\times^2} \quad (29)$$

This defines momentum dependent “effective masses” and widths, and a mixing parameter. The ratio of the “effective masses” to their vacuum values and the mixing parameter are shown on Fig. 9 for  $T = 0$  and  $n/n_{\text{sat}} = 0.1$ . Also shown on this figure are the dynamical masses, defined as the solution of the dispersion relation at zero 3-momentum  $k = (\omega_i^{\text{pl}}, \vec{0})$ :  $\mu_i^{\text{dyn}} = \omega_i^{\text{pl}}$ ,  $D(k) = 0$ . It can be seen that the mixing parameter deviates strongly from its vacuum value ( $= 1$ ) as long as the momentum transfer is lower than  $2 p_F$ . The transverse part of the  $\omega$  propagator remains almost unchanged. On the other hand, the “effective masses” of the  $\sigma$  and longitudinal part of the  $\omega$  follow the behavior of  $K_{\text{mix}}$ , the effective  $\sigma$  mass being reduced and the effective longitudinal  $\omega$  mass enhanced in the same proportion.

The mixing parameter comes as a multiplicative factor in  $G_\sigma$  and  $G_{\omega L}$ , so that the mixing could be absorbed in the redefinition of effective couplings for the  $\sigma$  and the longitudinal  $\omega$ , and be viewed as a weakening of the strength of these effective interactions.

Finally, the non-vanishing imaginary part of the polarizations which describes damping of the modes through particle-hole decay, contributes a positive term in the denominator of the square of the propagators and further reduces the value of the cross section in the medium.

---

<sup>3</sup>The condition  $\sqrt{-k^2} = 2 p_F$  is the same as that leading to the Kohn singularity at the threshold for particle-hole production which was at the origin of the Friedel oscillations in the  $N$ - $N$  potential [1].

It is now easy to understand the behavior of the differential cross-section at finite density. Since the momentum transfer is given in terms of the incident energy  $E = T_{lab} + M$  and scattering angle  $\theta$  by  $k^2 = -2(E^2 - M^2)(1 \pm \cos \theta)$ , the condition  $\sqrt{-k^2} < 2 p_F$  yields at constant energy the  $\theta$  range affected by medium effects:

$$|\cos \theta| > 1 - \frac{2p_F^2}{E^2 - M^2} \quad (30)$$

This corresponds to the range where  $d\sigma_{pp}/d\Omega$  becomes very forward peaked (and also backwards-peaked, since  $d\sigma_{pp}/d\Omega$  is symmetric by  $\theta \rightarrow \pi - \theta$ ).

## 5.2 Comparison with Brueckner calculations

The calculation we performed here amounts to consider loop contributions, while the Brueckner calculations of Li and Machleidt [16], Faessler *et al.* [11], Alm *et al.* [17] consider ladder contributions. In fact, both types of contributions should be included. This is however still somewhat beyond the present state of the art, as a naive ladder-resummation of our screened propagators would lead to inconsistencies (see *e.g.* a discussion in [52]).

Still it is interesting to study separately the effect of loops or ladders. The Brueckner resummation is expected to be more appropriate for low densities, since it is based on an expansion in  $na^3$  ( $a$  stands for the range of the interaction). On the other hand, our loop resummation is expected to be better at higher densities [53] and energies. In the case of the Brueckner resummation, the corrections due to finite density and temperature come in as Fermi factors on the intermediate (real) nucleon states on the uprights of the ladders, while in the case of loop resummations, the Fermi factors are applied on the intermediate (virtual) nucleon states forming the particle-hole loop. Both models, although they consider very different physical effects, lead to very similar results: decreasing  $\sigma_{pp}$  with increasing density and saturation for  $n > 2 n_{sat}$ , flattening over the energy range.

There are also some differences: we observe a modification of the in-medium cross section at high energies too, although the effect is smaller than at low energy. We also have a more rapid decrease with density for low values of  $n/n_{sat}$ . This result should probably not be taken too seriously: First, because, as already pointed out above, our model is not optimized for this range, and second, because these densities at  $T = 0$  fall within the domain of spinodal  $dP/d\rho < 0$  instability. Indeed, such a rapid variation of the cross section with the density is not observed when the background matter is heated moderately ( $T \sim 20$  MeV) so as to come out of the unphysical spinodal region.

## 5.3 Comparison with experimental constraints

During the last five years, it has become a general trend to investigate the influence of a modified  $N$ - $N$  cross section in the medium in numerical simulations in heavy ion collisions. We mention here, as a non-exhaustive sample, the work of Klakow *et al.* [4] or Alm *et al.* [8] on BUU codes, of Khoa *et al.* [9] on a QMD code, or of Tanaka *et al.* [54] with the antisymmetrized AMD code.

All these determinations are strongly model-dependent, but the fact that they all predict roughly the same effect, *i.e.* a 20 % reduction of the in-medium cross section at  $n = n_{sat}$ , although they rely on a very different physical analysis of the processes involved, sounds very encouraging.

We compare in Fig. 10 our results as well as the Brueckner results of Li and Machleidt [16] to the BUU prediction of Klakow *et al.* [4] as well as the AMD prediction of Tanaka *et al.* [54].

Tanaka *et al.* effected simulations of  $p$ +nucleus collisions using their antisymmetrized version of quantum molecular dynamics (AMD), and extracted a reduction factor for the in-medium  $N$ - $N$  cross section with respect to its free value by comparing the results of the simulation to available experimental data in the energy range [0 - 200] MeV. The  $p+{}^9\text{Be}$  collision probes low densities in the surface, while the  $p+{}^{12}\text{C}$ ,  $p+{}^{27}\text{Al}$ ,  $p+{}^{40}\text{Ca}$ , which all give similar results, are thought to probe the nuclear density  $n = n_{sat}$ . The result of Tanaka *et al.* is represented on Fig. 10 by triangles for  $p + {}^{40}\text{Ca}$  and diamonds for  $p + {}^9\text{Be}$ .

Klakow *et al.* estimated the medium-modified  $N - N$  cross section by performing simulations of heavy-ion collisions  $A + A$  with a Boltzmann-Uehling-Uhlenbeck transport model. The heavy ion collision takes place with an initial energy per nucleon 200 MeV and the system is evolved until freeze-out. The information on the cross section is obtained from an analysis of the dependence of nuclear transverse collective flow on beam energy, and the measurement of the so-called balance energy  $E_{bal}$  at which the flow disappears. This energy indicates a transition in which one goes from attractive to repulsive scattering. The authors assumed a density dependence  $\sigma_{med}/\sigma_{free} = 1 - \alpha(n/n_{sat})$  *i.e.* by taking the first order of a Taylor expansion at constant beam energy and zero temperature. The best agreement with experimental data was found to correspond to  $\alpha = 0.2$ . The result of Klakow *et al.* is shown on Fig. 10 by two arrows for densities  $n = 0.5 n_{sat}$  and  $n = n_{sat}$ .

The Brueckner calculation of Li and Machleidt [16] was described in the preceding paragraph. We display in Fig. 10 their result for the  $p$ - $p$  cross section at  $n = 0.5 n_{sat}$  (dotted line) and  $n = n_{sat}$  (continuous line).

Our results for the in-medium  $p$ - $p$  cross section are represented on Fig. 10 by four dashed and dot-dashed lines at densities  $n = 0.1n_{sat}$  and  $n = n_{sat}$  and for temperatures  $T = 0$  and  $T = 50$  MeV, as limiting values of what density and temperature conditions can be reached in the collisions considered by Klakow *et al.* or Tanaka *et al.*.

We can see that there is a fair overall agreement between these four approaches. Experimentally as well as theoretically, the cross section is found to be reduced with respect to its free value. There is also a qualitative agreement in the behavior with the beam energy: as the energy increases, the reduction factor decreases and saturates to a constant value. Both theoretical approaches (Brueckner, ours) overpredict the reduction of the  $N$ - $N$  cross section with respect to the experimental estimates. Two reasons may explain the observed discrepancies:

(i) The theoretical approaches consider that the collision is happening inside infinite nuclear matter, while in the experimental setup and the numerical simulations finite size effects play an important role, so that in a dynamical situation the dressing of the mesons may not be fully effective.

(ii) The calculation of Li and Machleidt as well as ours assume that the background matter is not far from local equilibrium, while the initial state of the collision is strongly out of equilibrium,



which also modifies the dressing of the mesons.

It is interesting to note that the discrepancies observed with the  $T=0$  calculations (Brueckner and ours) are reduced when finite temperatures are considered. This can be an indication that such finite temperature effects play a role in moderating the reduction of the cross section.

## (6) CONCLUSION AND OUTLOOK

### 6.1 Concluding summary

We have analyzed in this work some aspects of the screening effects on the nucleon-nucleon interaction, as due to the modifications introduced by the nuclear medium (at zero and finite temperature) on the propagation of the mesons which mediate this interaction. We applied here our results on dressed meson propagators to the calculation of the modification of proton-proton (or neutron-neutron) cross section for collisions occurring inside dense and hot nuclear matter. We found that the  $p$ - $p$  or  $n$ - $n$  total elastic cross sections were reduced with increasing density. The effect is more important at low energy, leading to a nearly constant cross section  $\sigma_{pp} \simeq 17$  mb at all energies for densities above the saturation value. The temperature dependence was found to be less pronounced, with first a slight increase and then a reduction with respect to the free value. The differential cross section becomes increasingly forward (and backward) peaked as the density or temperature grows.

The general features of the behavior with density are found to be the same as from a calculation with the Brueckner formalism effected by Li and Machleidt [16], although both approaches are very different. The reduction with density and its behavior with energy are compatible, although somewhat overestimated, with respect to the information extracted from BUU and AMD analysis of experimental data. Taking into account the effects of finite temperature in our approach seems to improve the agreement.

### 6.2 Improved meson exchange picture

While the calculation presented in this paper was restricted to the nucleon-nucleon scattering between identical particles through the exchange of  $\pi$ ,  $\sigma$  and  $\omega$  mesons, it is also possible to do the same for the neutron-proton cross section. In order to describe the  $T = 1$  isospin channel, it is necessary to consider also the exchange of the  $\rho$  meson. This calculation is presently under way, as well as the inclusion of the  $\eta$  and  $\delta$  mesons of the Bonn OBE potential.

Other interaction Lagrangians can be implemented using the same formalism, in particular with (non linear) meson interactions or chiral symmetry. A chiral symmetric interaction, although it is desirable from general considerations, has not yet reached the level of accuracy of the popular one-boson exchange picture in the description of  $N$ - $N$  scattering, so that we did not consider it in this work. This field however is in rapid evolution [56, 57, 58]. For example, the Nijmegen group [58] quote a value of  $\chi^2$  of 1.75 for a fit of the  $N$ - $N$  scattering data with 12 free parameters. It will bring a valuable piece of information to see how chirality modifies the behavior of the cross section, in particular in the high density or high temperature range where the chiral restoration takes place.

### 6.3 Background velocity

Also under consideration is the case when the background nuclear matter is moving with a non-zero velocity with respect to the center of mass of the collision. In this case, the behavior of the propagator in other regions of the  $\omega$ - $q$  plane will be explored. For a given value of the energy of the colliding particle and of the scattering angle, the values of the energy  $\omega$  and impulsion  $q$  entering the expression of the polarizations is given in section (3.2) as a function of the relative velocity. In particular (see Fig. 11), the region of the zero sound branches can be crossed. Such branches arise from the mixed  $\sigma$  - longitudinal  $\omega$  part of the dispersion relation [29, 32]. If  $(\omega, q)$  coincides with a zero-sound solution  $k_{zs}^\mu = (\omega_{zs}, q_{zs})$  of the dispersion relation

$$\left(k^2 - \mu_\sigma^2 + g_\sigma^2 \Pi_\sigma(k)\right) \left(k^2 - \mu_\omega^2 + g_\omega^2 \Pi_{\omega L}(k)\right) + g_\sigma g_\omega \Pi_\times^2(k) = 0, \quad (31)$$

there will be a critical value of the relative velocity  $v_{crit}$  for which the real part of the dispersion relation vanishes. For relative velocities near  $v_{crit}$  the real part of the dispersion, which appears in the denominator of the propagators, is reduced. As a consequence, the cross section will be enhanced.

A more detailed analysis of this and other effects of the relative velocity of the center of mass of the collision with respect to the background will be published separately.

### 6.4 $\Delta$ resonance

An important extension of the model should be the inclusion of the  $\Delta$  resonance. The  $\Delta$  and higher mass resonances will appear at several levels of the calculation: not only as the product of inelastic scattering processes, but also in a virtual  $\Delta$ -hole pair which will modify the propagation properties of the mesons and in particular of the pion. At high densities and temperature, the nuclear matter turns into the so-called resonance matter with a softer equation of state.

At the relativistic energies we are considering, a large number of  $\Delta(1232)$  are expected to be produced through the inelastic processes  $N + N \rightarrow \Delta + N$  and  $N + N \rightarrow \Delta + \Delta$ , and reabsorbed by the inverse reactions. In the vacuum, the inelastic channel begins to open for laboratory energies  $T_{lab} \geq 350$  MeV; at  $T_{lab} \geq 800$  MeV, the elastic and inelastic contributions to the total nucleon-nucleon cross section are roughly of the same size. The production *vs.* absorption rates of  $\Delta$  resonances is an important input in the calculation of the rapidity distributions  $dN_\pi/dy$  and  $dN_K/dy$  of the pions and kaons since these particles are produced through  $\Delta$  decays  $N + N \rightarrow N + \Delta \rightarrow N + N + \pi$  and  $N + N \rightarrow N + \Delta \rightarrow N + \Lambda + K$ . These distributions are the quantities actually accessible by experiment and are used to characterize the thermodynamical state of the piece of excited nuclear matter formed in a relativistic heavy ion collision. Scatterings  $N + \Delta \rightarrow N + \Delta$  will also contribute to the transport properties.

It is in principle straightforward to extend our formalism to calculate the  $N + N \rightarrow N + \Delta$  cross section once the dressed meson propagators are known. The  $\Delta$  is coupled to the nucleon through  $\Delta$ -N- $\pi$  and  $\Delta$ -N- $\rho$  vertices. The scattering matrix is obtained from terms such as

$$Tr[G_N(1)\Gamma_{\pi NN}G_N(3)\Gamma_{\pi NN}] Tr[G_N(2)\Gamma_{\pi N\Delta}G_\Delta(4)\Gamma_{\pi N\Delta}] D_\pi(31)D_\pi^*(31) \quad (32)$$

... *etc* and the  $\Delta$  decay width may in a first approximation be taken into account by integrating over a mass distribution function of the Breit-Wigner form. In this expression,  $G_N$  and  $G_\Delta$

are the dressed, on-shell propagators of the nucleon and  $\Delta$  respectively, and  $D_\pi$  is the screened pion propagator. Similar calculations were performed already (see *e.g.* [59] in the vacuum and [60, 61] with dressed pion propagators). Nevertheless, before doing this, we think that it is profitable to perform a more thorough study of the consequences of screened meson propagation on the nucleon-nucleon interaction on the example of elastic scattering.

Another way the presence of the  $\Delta$  can influence our calculations is in the description of the background nuclear matter. The  $\Delta$  can also appear in an internal line and contribute to the dressing of the mesons which mediate the interaction. It cannot be excluded that the corrections brought about by the creation of delta-hole loops in the propagators of the mesons might be sizable. But due to uncertainties and ambiguities in the description of the  $\Delta$ , a prediction at the quantitative level seems premature.

The quantum hadrodynamics Lagrangian of Serot and Walecka can be extended in order to include the  $\Delta$  resonance. The resulting (nonrenormalizable) Lagrangian (see *e.g.* [62]) introduces the  $\Delta$  with the Rarita-Schwinger spinor  $\Psi_\Delta^\mu$ . The  $\Delta$  interacts through the exchange of  $\sigma$  and  $\omega$  like the nucleons, moreover the  $\Delta$  couples to the nucleons through  $\Delta$ -N- $\pi$  and  $\Delta$ -N- $\rho$  vertices. A first uncertainty comes from the fact that the coupling constants of the  $\Delta$  to the  $\sigma$ ,  $\omega$  and  $\rho$  are not very well known, and there is not enough data to constrain these parameters. A more serious difficulty arises from the Rarita-Schwinger formalism itself. As a matter of fact, the propagator  $\Psi_\Delta^\mu \Psi_{\Delta\mu}$  contains not only spin 3/2 but also spin 1/2 parts. There has been a controversy whether or not one should project out the 1/2 part and how. When the  $\Delta$  is interacting, the theory becomes plagued by so-called off-shell ambiguities, *i.e.* new free parameters may be introduced at the vertices. Studies on the influence on the  $\Delta$  propagation noticed a strong dependence in these off-shell parameters [22].

There exists an abundant literature on the modification of the  $\pi$  dispersion relation by the  $\Delta$  (see *e.g.* [21, 22, 23]). This topic is not yet completely settled, especially concerning the relativistic treatment as discussed above. We have seen that the pion did not play a very important role in the proton-proton cross section. As a matter of fact, we checked this statement by simply replacing the dressed pion propagator by the free one, and observed a modification amounting to 5% at most. For the neutron-proton cross section nevertheless, the pion propagator will contribute a sizable part, as well as the  $\rho$ .

On the other hand, the modifications to the  $\sigma$  and  $\omega$  dispersion relations should be investigated in the case of  $pp$  scattering as well as for  $np$  scattering. Additional polarizations are given by terms such as:

$$\int d^4p \text{Tr}[G_\Delta(p+k/2)\Gamma_{\Delta\Delta\sigma}G_\Delta(p-k/2)\Gamma_{\Delta\Delta\sigma}] \quad (33)$$

As far as we know, the modification of other mesons than the pion by delta-hole loops has not yet been considered in the literature; this will need to be investigated in future work.

## 6.5 Form factors

The phenomenological form factors account for the fact that the nucleons are not pointlike, but have a quark gluon substructure. As a consequence, very high momentum transfer  $q$  would probe very short ranges at which our meson exchange picture fails. The cutoff suppresses these

unphysical contributions. The standard monopole form chosen in this work (see Eq. (18)) fits well the known data on the form factor in the vacuum.

At finite density and temperature, we kept this form factor unchanged according to our level of approximation. In fact, the form factor is expected to be modified in the medium: the nucleons “swell” (EMC effect) with increasing density. In a simple bag model picture, this is due to a reduced bag pressure. Higher order calculations of the vertex function [37], where the nucleon size is generated by a surrounding meson cloud, yield the same behavior. Higher momentum exchanges will thus be more strongly suppressed at higher density.

## APPENDIX A: Analytical formulae for the polarisations

Without loss of generality, the explicit form of the polarization terms can be given in the particular frame where  $k \equiv (\omega, 0, 0, q)$ . In this frame the only non-vanishing components of the polarizations are [29]:

$$\begin{aligned} & \Pi_{\sigma\omega}{}^0(k) ; \Pi_{\sigma\omega}{}^3(k) ; \Pi_{\omega}{}^{00}(k) ; \Pi_{\omega}{}^{03}(k) ; \Pi_{\omega}{}^{33}(k) ; \\ & \Pi_{\omega}{}^{11}(k) = \Pi_{\omega}{}^{22}(k) ; \Pi_{\sigma}(k) ; \Pi_{\pi}(k) \end{aligned} \quad (34)$$

The expressions of these components are directly obtained from

$$\Pi_{\sigma}(k) = 8\pi \int d^4p \left[ (p - k/2)(p + k/2) + M^2 \right] \cdot \Sigma(k, p) \quad (35)$$

$$\Pi_{\sigma\omega}{}^{\mu}(k) = 16\pi M \int d^4p p^{\mu} \cdot \Sigma(k, p) \quad (36)$$

$$\Pi_{\omega}{}^{\mu\nu}(k) = 16\pi \int d^4p \left[ p^{\mu}p^{\nu} - k^{\mu}k^{\nu}/4 - (1/2)(p^2 - k^2/4 - M^2)g^{\mu\nu} \right] \cdot \Sigma(k, p) \quad (37)$$

$$\Pi_{\pi}(k) = 8\pi \int d^4p \left[ (p - k/2)(p + k/2) - M^2 \right] \cdot \Sigma(k, p) \quad (38)$$

where

$$\Sigma(k, p) = [f(p + k/2) - f(p - k/2)] / (k \cdot p - i\epsilon) \quad (39)$$

and the  $i\epsilon$  term comes from the boundary prescription for the fermionic dressed propagator which enters the loop expressions of the polarizations. It gives the imaginary parts of these polarizations through the well know formula  $1/(x - i\epsilon) = \mathcal{P}/x + i\pi\delta(x)$ , where  $\mathcal{P}$  is the principal part. The fermion distribution function  $f(p)$  in (39) is given by

$$f(p) = (2\pi)^{-3} \delta(p^2 - M^2). [\Omega^+ + \Omega^- - H(-p_0)] \quad (40)$$

the  $\Omega$ 's are the Fermi factors defined as :

$$\Omega^\pm = H(\pm p_0). \{1 + \exp(\beta[E(\vec{p}) \mp \mu])\}^{-1} \quad (41)$$

and  $H(x)$  is the Heaviside step function.  $\beta$  is the inverse temperature and  $\mu$  is the auxiliary chemical potential, related to the true chemical potential by  $\mu_{true} = \mu - g_\omega \omega_0$ . The quasi-particles are on the mass-shell:

$$M = m - g_\sigma \sigma \quad E(\vec{p}) = \sqrt{(\vec{p}^2 + M^2)} \quad (42)$$

### A.1 Real part of polarization tensors

The matter contributions to the real part of the polarization tensors is immediately obtained from Eqs. (35) to (38) by excluding the last term in Eqs. (40). This last term corresponds to the quasi-nucleon distribution in the Dirac sea (vacuum distribution) and leads to divergences in the calculation of the real parts of the polarization tensors which must be renormalized. For the real part of the scalar polarization  $\Pi_\sigma(k)$ , the renormalized vacuum contribution has been obtained as usually, by regularizing the infinite vacuum polarization (which contains divergences proportional to  $k^2$ ,  $\sigma$  and  $\sigma^2$ ) and adding to the Lagrangian the counterterms which allow to cancel such divergences. The finite undefined constants in the renormalized expression are determined by imposing a on-mass-shell criterion to the real renormalized dispersion relation for the scalar mesons at vanishing density [29]. The final form of the vacuum finite (*v.f.*) part of the scalar polarization is

$$\begin{aligned} \Pi_{\sigma v f}(k) &= (2k^2 - 8m^2)\theta_\sigma + 8(M^2 - k^2/4)\theta(k^2, M^2) \\ &+ 8(m^2 - \mu_\sigma^2/4)(\mu_\sigma^2 - k^2)\theta_{\sigma k} + (6M^2 - k^2) \ln(M/m)^2 \\ &- 2g^2\sigma^2 [6 + \mu_\sigma^2/m^2 + 16m^2\theta_{\sigma m} + 8(m^2 - \mu_\sigma^2/4)m^2\theta_{\sigma m m}] \\ &- (M^2 - m^2) [6 - \mu_\sigma^2/m^2 + 8\theta_\sigma + 8(m^2 - \mu_\sigma^2/4)\theta_{\sigma m}] \end{aligned} \quad (43)$$

and the function  $\theta(k^2, M^2)$  is given by the integral:

$$\theta(k^2, M^2) = \theta(y) = y \int_0^\infty dx / [(x^2 + y) \cdot \sqrt{(x^2 + 1)}] \quad (44)$$

with :

$$y \equiv 1 - k^2/(4M^2).$$

In writing down Eq. (43), we have introduced the notations:

$$\begin{aligned}
\theta_\sigma &= \theta(\mu_\sigma^2, m^2), \\
\theta_{\sigma m} &= \partial\theta(k^2, M^2)/\partial M^2, \\
\theta_{\sigma k} &= \partial\theta(k^2, M^2)/\partial k^2 \\
\theta_{\sigma mm} &= \partial^2\theta(k^2, M^2)/\partial(M^2)^2.
\end{aligned} \tag{45}$$

All these derivatives are to be calculated at the point  $k^2 = \mu_\sigma^2, M = m$ .

As it can easily be seen, there is no vacuum contribution to the mixing polarization part  $\Pi_{\sigma\omega}{}^\mu(k)$ .

The finite vacuum contributions to the vector polarization tensor  $\Pi_\omega{}^{\mu\nu}(k)$ , is obtained from Eq.(37) using dimensional regularization and compensating the divergent contributions through the appropriate counterterms [29]. The final expression is

$$\Pi_{\omega\nu f}{}^{\mu\nu}(k) = (4/3\pi) [k^2 \ln(M/m) - 2M^2 + (2M^2 + k^2)\theta(k^2, M^2) + \Gamma] \Delta^{\mu\nu}(k) \tag{46}$$

where the projector  $\Delta^{\mu\nu}(k)$  is defined by:

$$\Delta^{\mu\nu}(k) = g^{\mu\nu} - k^\mu k^\nu / k^2 \tag{47}$$

Here  $\theta(k^2, M^2)$  is the same function defined in Eq. (44) and  $\Gamma$  is a finite constant which, determined through the on-shell renormalization conditions, becomes:

$$\Gamma = 2m^2 - (2m^2 + \mu_\omega^2)\theta(\mu_\omega^2, m^2) \tag{48}$$

The renormalized vacuum contributions to the real part of the pion polarization obtained from the same on-shell prescription is [29]

$$\begin{aligned}
\Pi_{\pi\nu f}(k) &= 2k^2 [\theta_\pi - \theta(k^2, M^2) + \mu_\pi^2 \theta_{\pi k}] - 2\mu_\pi^4 \theta_{\pi k} \\
&+ (2M^2 - k^2) \ln(M/m)^2 - (2 - \mu_\pi^2/m^2 - 2\mu_\pi^2 \theta_{\pi m}) (M^2 - m^2) \\
&- 2g^2 \sigma^2 (2 + \mu_\pi^2/m^2 - 2\mu_\pi^2 m^2 \theta_{\pi mm})
\end{aligned} \tag{49}$$

where the definition of the derivatives of the functions  $\theta$  is the same as in Eqs. (44) with the replacement of  $\mu_\sigma$  by  $\mu_\pi$ .

## A.2 Imaginary part of polarization tensors.

The only non-vanishing components of the imaginary parts of the polarization tensors are:

$$\Pi_{\pi,I}(k) \quad ; \quad (50)$$

$$\Pi_{\sigma,I}(k) \quad ; \quad (51)$$

$$\Pi_{\sigma\omega,I}^3(k) = (\omega/q)\Pi_{\sigma\omega,I}^0(k) ; \quad (52)$$

$$\Pi_{\omega,I}^{33}(k) = (\omega/q)\Pi_{\omega,I}^{03}(k) = (\omega^2/q^2)\Pi_{\omega,I}^{00}(k) ; \quad (53)$$

$$\Pi_{\omega,I}^{11}(k) = \Pi_{\omega,I}^{22}(k) \quad (54)$$

the relations between the vector-mixing and tensor components being a consequence of the baryonic charge conservation. The expression for the finite temperature imaginary part of the scalar polarization is:

$$\Pi_{\sigma,I}(\omega, q) = \Delta(\omega^2 - q^2)/q \int_M^\infty dE [H(A^+) - H(A^-)] [\Omega^+ - \Omega^- - 1] \quad (55)$$

where

$$A^\pm = q\sqrt{E^2 - M^2} - |\omega E \pm (\omega^2 - q^2)/2| \quad (56)$$

$$\Omega^\pm = \{1 + \exp(\beta[E \mp \mu])\}^{-1} \quad (57)$$

$$\Delta = 1 - 4M^2/(\omega^2 - q^2) \quad (58)$$

The three terms inside brackets in Eq. (55) correspond respectively to the contributions of baryons, antibaryons and vacuum. Here and in the next formulae the vacuum contributions are finite.

The imaginary part of the pion polarization is obtained from the imaginary part of the  $\sigma$  polarization through

$$\Pi_{\pi,I}(\omega, q) = \Pi_{\sigma,I}(\omega, q)/\Delta \quad (59)$$

The independent imaginary component of the mixing polarization vector is

$$\Pi_{\sigma\omega,I}^0(\omega, q) = \frac{4M}{q} \int_M^\infty dE \left[ \left(E - \frac{\omega}{2}\right) H(A^-) - \left(E + \frac{\omega}{2}\right) H(A^+) \right] (\Omega^+ + \Omega^-) \quad (60)$$

where the vacuum contributions vanish.

The independent imaginary components of the  $\omega$  polarization tensor are

$$\begin{aligned} \Pi_{\omega,I}^{00}(\omega, q) &= \frac{4}{q} \int_M^\infty dE \left\{ \left[ \left( E - \frac{\omega}{2} \right)^2 - \frac{q^2}{4} \right] H(A^-) - \left[ \left( E + \frac{\omega}{2} \right)^2 - \frac{q^2}{4} \right] H(A^+) \right\} \\ &\quad \times (\Omega^+ - \Omega^- + 1) \end{aligned} \quad (61)$$

and

$$\begin{aligned} \Pi_{\omega,I}^{11}(\omega, q) &= \frac{2}{q} \int_M^\infty dE \left\{ \left[ \left( E - \frac{\omega}{2} \right) \left( 1 - \frac{\omega^2}{q^2} \right) - M^2 \right] H(A^-) \right. \\ &\quad \left. - \left[ \left( E + \frac{\omega}{2} \right) \left( 1 - \frac{\omega^2}{q^2} \right) - M^2 \right] H(A^+) \right\} (\Omega^+ - \Omega^- + 1) \end{aligned} \quad (62)$$

## APPENDIX B: Analytical expression of the cross section

The expression of the spin-averaged nucleon-nucleon cross section results from taking the square of the transition matrix Eq. (19) and using the relation  $\sum_s u(p, s) \bar{u}(p, s) = \gamma \cdot p + m$ . We use the short notation  $S_i = \gamma \cdot p_{i*} + m_*$ .

The calculation of the transition matrix is straightforward. We give here the result as a function of the Mandelstam variables and of the relative background velocity. Additional terms appear due to  $\sigma$ - $\omega$  mixing, for example for the direct term:

$$\begin{aligned} |\overline{\mathcal{M}}|^2 &\ni \frac{g_\sigma^2 g_\omega^2}{4} \left\{ \mathcal{F}_\sigma^2(k_{31*}) \mathcal{F}_\omega^2(k_{31*}) (\text{Tr}[S_3 \gamma_\mu S_1 \gamma_\alpha] \text{Tr}[S_4 S_2] \right. \\ &\quad + \text{Tr}[S_3 \gamma_\mu S_1] \text{Tr}[S_4 S_2 \gamma_\alpha] + \text{Tr}[S_3 S_1 \gamma_\alpha] \text{Tr}[S_4 \gamma_\mu S_2] \\ &\quad \left. + \text{Tr}[S_3 S_1] \text{Tr}[S_4 \gamma_\mu S_2 \gamma_\alpha]) G_{\sigma\omega}^\mu(k_{31*}) G_{\sigma\omega}^\alpha(k_{31*})^* \right. \\ &+ \frac{g_\sigma^3 g_\omega}{4} \left\{ \mathcal{F}_\sigma^3(k_{31*}) \mathcal{F}_\omega^2(k_{31*}) (\text{Tr}[S_3 S_1 \gamma_\alpha] \text{Tr}[S_4 S_2] \right. \\ &\quad + \text{Tr}[S_3 S_1] \text{Tr}[S_4 S_2 \gamma_\alpha]) G_\sigma(k_{31*}) G_{\sigma\omega}^\alpha(k_{31*})^* \\ &\quad + \mathcal{F}_\sigma^3(k_{31*}) \mathcal{F}_\omega^2(k_{31*}) (\text{Tr}[S_3 \gamma_\alpha S_1] \text{Tr}[S_4 S_2] \\ &\quad \left. + \text{Tr}[S_3 S_1] \text{Tr}[S_4 S_2 \gamma_\alpha]) G_\sigma(k_{31*})^* G_{\sigma\omega}^\alpha(k_{31*}) \right\} \\ &+ \frac{g_\sigma g_\omega^3}{4} \left\{ \mathcal{F}_\sigma(k_{31*}) \mathcal{F}_\omega^3(k_{31*}) (\text{Tr}[S_3 \gamma_\mu S_1 \gamma_\alpha] \text{Tr}[S_4 \gamma_\nu S_2] \right. \\ &\quad + \text{Tr}[S_3 \gamma_\mu S_1] \text{Tr}[S_4 \gamma_\nu S_2 \gamma_\alpha]) G_\omega^{\mu\nu}(k_{31*}) G_{\sigma\omega}^\alpha(k_{31*})^* \\ &\quad + \mathcal{F}_\sigma(k_{31*}) \mathcal{F}_\omega^3(k_{31*}) (\text{Tr}[S_3 \gamma_\alpha S_1 \gamma_\nu u] \text{Tr}[S_4 S_2 \gamma_\mu] \\ &\quad \left. + \text{Tr}[S_3 S_1 \gamma_\nu] \text{Tr}[S_4 \gamma_\alpha S_2 \gamma_\mu]) G_\omega^{\mu\nu}(k_{31*})^* G_{\sigma\omega}^\alpha(k_{31*}) \right\} \\ &+ \frac{g_\sigma g_\omega g_\pi^2}{4} \left\{ \mathcal{F}_\sigma(k_{31*}) \mathcal{F}_\omega(k_{31*}) \mathcal{F}_\pi^2(k_{31*}) (\text{Tr}[S_3 \gamma_\mu S_1 \gamma_5] \text{Tr}[S_4 S_2 \gamma_5] \right. \\ &\quad + \text{Tr}[S_3 S_1 \gamma_5] \text{Tr}[S_4 \gamma_\mu S_2 \gamma_5]) G_{\sigma\omega}^\mu(k_{31*}) G_\pi(k_{31*})^* \\ &\quad + \mathcal{F}_\sigma(k_{31*}) \mathcal{F}_\omega(k_{31*}) \mathcal{F}_\pi^2(k_{31*}) (\text{Tr}[S_3 \gamma_5 S_1 \gamma_\mu] \text{Tr}[S_4 \gamma_5 S_2] \\ &\quad \left. + \text{Tr}[S_3 \gamma_5 S_1] \text{Tr}[S_4 \gamma_5 S_2 \gamma_\mu]) G_{\sigma\omega}^\mu(k_{31*})^* G_\pi(k_{31*}) \right\} \end{aligned}$$



In this formula, the  $\mathcal{F}(k)$  are the form factors given by Eq. (18) and  $k_{31}$  is the quadrivector for momentum transfer in the direct diagram  $k_{31}^\mu = p_{1*}^\mu - p_{3*}^\mu$ .

The Mandelstam variables are related to the incident  $p_{1*}, p_{2*}$  and outgoing  $p_{3*}, p_{4*}$  impulses by

$$s = (p_{1*} + p_{2*})^2 \quad (63)$$

$$t = (p_{1*} - p_{3*})^2 \quad (64)$$

$$u = (p_{1*} - p_{4*})^2 \quad (65)$$

with  $s + t + u = 4 m_*^2$ .

When the incident and outgoing particles are on their effective mass-shell  $p_{i*}^2 = m_*^2$ , and if take into account the energy momentum conservation  $p_{1*}^\mu + p_{2*}^\mu = p_{3*}^\mu + p_{4*}^\mu$ , we have

$$s = 2 (m_*^2 + p_{1*} \cdot p_{2*}) = 4 E^2 \quad (66)$$

$$t = 2 (m_*^2 - p_{1*} \cdot p_{3*}) = 2 (m_*^2 - E^2)(1 - \cos \theta) \quad (67)$$

$$u = 2 (m_*^2 - p_{1*} \cdot p_{4*}) = 2 (m_*^2 - E^2)(1 + \cos \theta) \quad (68)$$

If the relative velocity between the background nuclear matter and the center of mass of the collision  $u^\mu = (\gamma, \gamma v \sin \alpha \cos \varphi, \gamma v \sin \alpha \cos \varphi, \gamma v \cos \alpha)$  is finite, and when calculating terms containing the longitudinal part of the vector meson propagator, we will also have components along the vectors

$$\eta_\ominus^\mu = u^\mu - \frac{\eta \cdot u}{q_{31}^2} q_{31}^\mu \quad \text{and} \quad \eta_\oplus^\mu = u^\mu - \frac{\eta \cdot u}{q_{41}^2} q_{41}^\mu$$

We note the projections of the particle momenta on these directions  $p_1^\ominus = p_1^\mu \cdot \eta_{\ominus\mu}$ , etc. They are related to the Mandelstam variables defined above and to the components of the relative velocity through

$$p_1^\ominus = p_3^\ominus = \sqrt{\frac{t}{t - \omega_\ominus^2}} \left[ \gamma \sqrt{\frac{s}{4}} - \gamma v \cos \alpha \sqrt{\frac{s}{4} - m_*^2} - \frac{\omega_\ominus}{2} \right]$$

$$p_2^\ominus = p_4^\ominus = \sqrt{\frac{t}{t - \omega_\ominus^2}} \left[ \gamma \sqrt{\frac{s}{4}} + \gamma v \cos \alpha \sqrt{\frac{s}{4} - m_*^2} + \frac{\omega_\ominus}{2} \right]$$

$$p_1^\oplus = p_4^\oplus = \sqrt{\frac{u}{u - \omega_\oplus^2}} \left[ \gamma \sqrt{\frac{s}{4}} - \gamma v \cos \alpha \sqrt{\frac{s}{4} - m_*^2} - \frac{\omega_\oplus}{2} \right]$$

$$p_2^\oplus = p_3^\oplus = \sqrt{\frac{u}{u - \omega_\oplus^2}} \left[ \gamma \sqrt{\frac{s}{4}} + \gamma v \cos \alpha \sqrt{\frac{s}{4} - m_*^2} + \frac{\omega_\oplus}{2} \right]$$

The  $\omega_\ominus$  and  $\omega_\oplus$  were defined in section (3.2). In terms of the Mandelstam variables,

$$\omega_\ominus = \gamma v \sqrt{\frac{s}{4} - m_*^2} \left[ \sin \alpha \sin \varphi \sqrt{1 - \left( \frac{t-u}{s} \right)} - \cos \alpha \left( 1 - \frac{t-u}{s} \right) \right]$$

$$\omega_\oplus = \gamma v \sqrt{\frac{s}{4} - m_*^2} \left[ -\sin \alpha \sin \varphi \sqrt{1 - \left( \frac{t-u}{s} \right)} - \cos \alpha \left( 1 + \frac{t-u}{s} \right) \right]$$

We split for convenience here the propagator of the  $\omega$  vector mesons in a transverse part  $G_{\omega T}$  and a part along the vector  $\eta$ :  $G_{\omega N}(t) = G_{\omega L}(t) - G_{\omega T}(t)$ .

The spin-averaged scattering matrix for the Coulomb subtracted elastic nucleon-nucleon scattering is given by:

$$\begin{aligned} \frac{d\sigma_{pp}}{d\Omega} &= \frac{d\sigma_{nn}}{d\Omega} \\ &= \frac{1}{64\pi^2 s} [\mathcal{S}_{4\sigma} + \mathcal{S}_{4\omega} + \mathcal{S}_{2\sigma 2\omega} + \mathcal{S}_{1\sigma 3\omega} + \mathcal{S}_{3\sigma 1\omega} + \mathcal{S}_{4\pi} + \mathcal{S}_{2\pi 2\sigma} + \mathcal{S}_{2\pi 2\omega} + \mathcal{S}_{2\pi 1\sigma 1\omega}] \end{aligned} \quad (69)$$

with ( $e$ ,  $d$  and  $i$  are the direct, exchange and interference terms)

$$\begin{aligned} \mathcal{S}_{4\sigma} &= \mathcal{S}_{4\sigma}^d + \mathcal{S}_{4\sigma}^e + \mathcal{S}_{4\sigma}^i \\ \mathcal{S}_{4\sigma}^d &= g_\sigma^4 \mathcal{F}_\sigma^4(t) \left[ (4m_*^2 - t)^2 \right] G_\sigma(t) G_\sigma^*(t) \\ \mathcal{S}_{4\sigma}^e &= g_\sigma^4 \mathcal{F}_\sigma^4(u) \left[ (4m_*^2 - u)^2 \right] G_\sigma(u) G_\sigma^*(u) \\ \mathcal{S}_{4\sigma}^i &= -g_\sigma^4 \mathcal{F}_\sigma^2(t) \mathcal{F}_\sigma^2(u) \left[ \frac{t^2 + u^2 - s^2}{4} + 4m_*^2(s - m_*^2) \right] \cdot \{G_\sigma(t) G_\sigma^*(u) + G_\sigma^*(t) G_\sigma(u)\} \\ \\ \mathcal{S}_{4\omega} &= \mathcal{S}_{4\omega}^d + \mathcal{S}_{4\omega}^e + \mathcal{S}_{4\omega}^i \\ \mathcal{S}_{4\omega}^d &= g_\omega^4 \mathcal{F}_\omega(t)^4 \left( 4 \left[ (s - u)^2 + t(t + 8m_*^2) \right] \cdot \{G_{\omega T}(t) G_{\omega T}^*(t)\} \right. \\ &\quad + 4 \left[ 4t(p_{1\ominus}^2 + p_{4\ominus}^2) + 16p_{1\ominus}^2 p_{4\ominus}^2 + t^2 \right] \{G_{\omega N}(t) G_{\omega N}^*(t)\} \\ &\quad + 4 \left[ 4(s - u)p_{1\ominus} p_{4\ominus} + 4t(p_{1\ominus}^2 + p_{4\ominus}^2) + t^2 \right] \times \\ &\quad \left. \times \{G_{\omega N}(t) G_{\omega T}^*(t) + G_{\omega N}^*(t) G_{\omega T}(t)\} \right) \\ \mathcal{S}_{4\omega}^e &= g_\omega^4 \mathcal{F}_\omega(u)^4 \left( 4 \left[ (s - t)^2 + u(u + 8m_*^2) \right] \cdot \{G_{\omega T}(u) G_{\omega T}^*(u)\} \right. \\ &\quad + 4 \left[ 4u(p_{1\oplus}^2 + p_{4\oplus}^2) + 16p_{1\oplus}^2 p_{4\oplus}^2 + u^2 \right] \{G_{\omega N}(u) G_{\omega N}^*(u)\} \\ &\quad + 4 \left[ 4(s - t)p_{1\oplus} p_{4\oplus} + 4u(p_{1\oplus}^2 + p_{4\oplus}^2) + u^2 \right] \times \\ &\quad \left. \times \{G_{\omega N}(u) G_{\omega T}^*(u) + G_{\omega N}^*(u) G_{\omega T}(u)\} \right) \\ \mathcal{S}_{4\omega}^i &= g_\omega^4 \mathcal{F}_\omega^2(u) \mathcal{F}_\omega^2(t) \left( - \left[ 8(s - 2m_*^2)(6m_*^2 - s) \right] \cdot \{G_{\omega T}(t) G_{\omega T}^*(u) + G_{\omega T}^*(t) G_{\omega T}(u)\} \right. \\ &\quad - \left[ 8(4m_*^2 - s)(p_{1\ominus} p_{4\ominus} + p_{1\oplus} p_{3\oplus}) - 4t(p_{1\ominus}^2 + p_{4\ominus}^2) - 4u(p_{1\oplus}^2 + p_{3\oplus}^2) \right. \\ &\quad \left. + 32p_{1\ominus} p_{4\ominus} p_{1\oplus} p_{3\oplus} - 2ut(2\eta_\ominus \cdot \eta_\oplus - 1) \right] \times \\ &\quad \left. \times \{G_{\omega N}(t) G_{\omega N}^*(u) + G_{\omega N}^*(t) G_{\omega N}(u)\} \right. \\ &\quad - \left[ 4s(p_{1\oplus} - p_{3\oplus})^2 - 8u(p_{1\oplus}^2 + p_{3\oplus}^2) + 4t(p_{1\oplus} + p_{3\oplus})^2 - 8um_*^2 \right. \\ &\quad \left. - 16m_*^2(p_{1\oplus}^2 + p_{3\oplus}^2 - 4p_{1\oplus} p_{3\oplus}) - 2(s - 2m_*^2)(s - u) + 2(2m_*^2 - t)(4m_*^2 - t) \right] \end{aligned}$$

$$\begin{aligned}
& + 2ut\left(1 + \frac{2}{t}(p_{1\oplus} - p_{3\oplus})^2\right) \left\{ G_{\omega N}(u)G_{\omega T}^*(t) + G_{\omega N}^*(u)G_{\omega T}(t) \right\} \\
& - \left[ 4s(p_{1\ominus} - p_{4\ominus})^2 - 8t(p_{1\ominus}^2 + p_{4\ominus}^2) + 4u(p_{1\ominus} + p_{4\ominus})^2 - 8tm_*^2 \right. \\
& - 16m_*^2(p_{1\ominus}^2 + p_{4\ominus}^2 - 4p_{1\ominus}p_{4\ominus}) - 2(s - 2m_*^2)(s - t) + 2(2m_*^2 - u)(4m_*^2 - u) \\
& \left. + 2ut\left(1 + \frac{2}{u}(p_{1\ominus} - p_{4\ominus})^2\right) \right] \left\{ G_{\omega N}(t)G_{\omega T}^*(u) + G_{\omega N}^*(t)G_{\omega T}(u) \right\}
\end{aligned}$$

$$\mathcal{S}_{2\sigma 2\omega} = \mathcal{S}_{2\sigma 2\omega}^d + \mathcal{S}_{2\sigma 2\omega}^e + \mathcal{S}_{2\sigma 2\omega}^i$$

$$\begin{aligned}
\mathcal{S}_{2\sigma 2\omega}^d &= g_\sigma^2 g_\omega^2 \mathcal{F}_\sigma^2(t) \mathcal{F}_\omega^2(t) \left( [-16m_*^2(s - u)] \cdot \{ G_\sigma(t)G_{\omega T}^*(t) + G_\sigma^*(t)G_{\omega T}(t) \} \right. \\
& + [-64m_*^2 p_{1\oplus} p_{4\oplus}] \cdot \{ G_\sigma(t)G_{\omega N}^*(t) + G_\sigma^*(t)G_{\omega N}(t) \} \\
& \left. + \left[ 16(4m_*^2 - t)\left(\frac{t}{2} + p_{1\ominus}^2 + p_{4\ominus}^2\right) + 128m_*^2 p_{1\oplus} p_{4\oplus} \right] \cdot \{ G_\times(t)G_\times^*(t) \} \right)
\end{aligned}$$

$$\begin{aligned}
\mathcal{S}_{2\sigma 2\omega}^e &= g_\sigma^2 g_\omega^2 \mathcal{F}_\sigma^2(u) \mathcal{F}_\omega^2(u) \left( [-16m_*^2(s - t)] \cdot \{ G_\sigma(u)G_{\omega T}^*(u) + G_\sigma^*(u)G_{\omega T}(u) \} \right. \\
& + [-64m_*^2 p_{1\oplus} p_{3\oplus}] \cdot \{ G_\sigma(u)G_{\omega N}^*(u) + G_\sigma^*(u)G_{\omega N}(u) \} \\
& \left. + \left[ 16(4m_*^2 - u)\left(\frac{u}{2} + p_{1\oplus}^2 + p_{3\oplus}^2\right) + 128m_*^2 p_{1\oplus} p_{3\oplus} \right] \cdot \{ G_\times(u)G_\times^*(u) \} \right)
\end{aligned}$$

$$\begin{aligned}
\mathcal{S}_{2\sigma 2\omega}^i &= g_\sigma^2 g_\omega^2 \mathcal{F}_\sigma^2(t) \mathcal{F}_\omega^2(u) \left( \left[ 4(24m_*^2 - 4m_*^2 s - 10m_*^2 t + t^2) \right] \cdot \{ G_\sigma(t)G_{\omega T}^*(u) + G_\sigma^*(t)G_{\omega T}(u) \} \right. \\
& + \left[ 2u(s + u) + 4u(p_{1\oplus}^2 + p_{3\oplus}^2) + 8sp_{1\oplus} p_{3\oplus} \right] \times \\
& \quad \times \{ G_\sigma(t)G_{\omega N}^*(u) + G_\sigma^*(t)G_{\omega N}(u) \} \\
& + g_\sigma^2 g_\omega^2 \mathcal{F}_\sigma^2(u) \mathcal{F}_\omega^2(t) \left( \left[ 4(24m_*^2 - 4m_*^2 s - 10m_*^2 u + u^2) \right] \cdot \{ G_\sigma(u)G_{\omega T}^*(t) + G_\sigma^*(u)G_{\omega T}(t) \} \right. \\
& + \left[ 2t(s + t) + 4t(p_{1\ominus}^2 + p_{4\ominus}^2) + 8sp_{1\ominus} p_{4\ominus} \right] \times \\
& \quad \times \{ G_\sigma(u)G_{\omega N}^*(t) + G_\sigma^*(u)G_{\omega N}(t) \} \\
& - g_\sigma^2 g_\omega^2 \mathcal{F}_\sigma(t) \mathcal{F}_\sigma(u) \mathcal{F}_\omega(u) \mathcal{F}_\omega(t) \left[ 32m_*^2(p_{1\ominus} + p_{4\ominus})(p_{1\oplus} + p_{3\oplus}) + 8ut \eta_\ominus \eta_\oplus \right] \times \\
& \quad \times \{ G_\times(u)G_\times^*(t) + G_\times^*(u)G_\times(t) \}
\end{aligned}$$

$$\mathcal{S}_{1\sigma 3\omega} = \mathcal{S}_{1\sigma 3\omega}^d + \mathcal{S}_{1\sigma 3\omega}^e + \mathcal{S}_{1\sigma 3\omega}^i$$

$$\begin{aligned}
\mathcal{S}_{1\sigma 3\omega}^d &= g_\sigma g_\omega^3 \mathcal{F}_\sigma(t) \mathcal{F}_\omega^3(t) \left( [32m_*((s - u)p_{1\oplus} + tp_{4\oplus})] \cdot \{ G_\times(t)G_{\omega T}^*(t) + G_\times^*(t)G_{\omega T}(t) \} \right. \\
& \left. + [16m_*(p_{1\ominus} + p_{4\ominus})(t + 4p_{1\oplus} p_{4\oplus})] \cdot \{ G_\times(t)G_{\omega N}^*(t) + G_\times^*(t)G_{\omega N}(t) \} \right)
\end{aligned}$$

$$\begin{aligned}
\mathcal{S}_{1\sigma 3\omega}^e &= g_\sigma g_\omega^3 \mathcal{F}_\sigma(u) \mathcal{F}_\omega^3(u) \left( [32m_*((s - t)p_{1\oplus} + up_{3\oplus})] \cdot \{ G_\times(u)G_{\omega T}^*(u) + G_\times^*(u)G_{\omega T}(u) \} \right. \\
& \left. + [16m_*(p_{1\oplus} + p_{3\oplus})(u + 4p_{1\oplus} p_{3\oplus})] \cdot \{ G_\times(u)G_{\omega N}^*(u) + G_\times^*(u)G_{\omega N}(u) \} \right)
\end{aligned}$$

$$\begin{aligned}
\mathcal{S}_{1\sigma 3\omega}^i &= -g_\sigma g_\omega^3 \mathcal{F}_\sigma(t) \mathcal{F}_\omega(t) \mathcal{F}_\omega^2(u) \left( \left[ 16m_*(p_{1\ominus} + p_{4\ominus})(u - t + 2m_*^2) \right] \cdot \{G_\times(t) G_{\omega T}^*(u) + G_\times^*(t) G_{\omega T}(u)\} \right. \\
&\quad \left. + [8m_*(p_{1\ominus} + p_{4\ominus})(4p_{1\oplus} p_{3\oplus} + u)] \cdot \{G_\times(t) G_{\omega N}^*(u) + G_\times^*(t) G_{\omega N}(u)\} \right) \\
&\quad - g_\sigma g_\omega^3 \mathcal{F}_\sigma(u) \mathcal{F}_\omega(u) \mathcal{F}_\omega^2(t) \left( \left[ 16m_*(p_{1\oplus} + p_{3\oplus})(t - u + 2m_*^2) \right] \cdot \{G_\times(u) G_{\omega T}^*(t) + G_\times^*(u) G_{\omega T}(t)\} \right. \\
&\quad \left. + [8m_*(p_{1\oplus} + p_{3\oplus})(4p_{1\ominus} p_{4\ominus} + t)] \cdot \{G_\times(u) G_{\omega N}^*(t) + G_\times^*(u) G_{\omega N}(t)\} \right)
\end{aligned}$$

$$\mathcal{S}_{3\sigma 1\omega} = \mathcal{S}_{3\sigma 1\omega}^d + \mathcal{S}_{3\sigma 1\omega}^e + \mathcal{S}_{3\sigma 1\omega}^i$$

$$\begin{aligned}
\mathcal{S}_{3\sigma 1\omega}^d &= -g_\sigma^3 g_\omega \mathcal{F}_\sigma^3(t) \mathcal{F}_\omega(t) \left[ 16m_*(4m_*^2 - t)(p_{1\ominus} + p_{4\ominus}) \right] \cdot \{G_\times(t) G_\sigma^*(t) + G_\times^*(t) G_\sigma(t)\} \\
\mathcal{S}_{3\sigma 1\omega}^e &= -g_\sigma^3 g_\omega \mathcal{F}_\sigma^3(u) \mathcal{F}_\omega(u) \left[ 16m_*(4m_*^2 - u)(p_{1\oplus} + p_{3\oplus}) \right] \cdot \{G_\times(u) G_\sigma^*(u) + G_\times^*(u) G_\sigma(u)\} \\
\mathcal{S}_{3\sigma 1\omega}^i &= g_\sigma^3 g_\omega \left( \mathcal{F}_\sigma^2(t) \mathcal{F}_\sigma(u) \mathcal{F}_\omega(u) \left[ 8m_*(4m_*^2 - t)(p_{1\oplus} + p_{3\oplus}) \right] \cdot \{G_\sigma(t) G_\times^*(u) + G_\sigma^*(t) G_\times(u)\} \right. \\
&\quad \left. + \mathcal{F}_\sigma^2(u) \mathcal{F}_\sigma(t) \mathcal{F}_\omega(t) \left[ 8m_*(4m_*^2 - u)(p_{1\ominus} + p_{4\ominus}) \right] \cdot \{G_\sigma(u) G_\times^*(t) + G_\sigma^*(u) G_\times(t)\} \right)
\end{aligned}$$

$$\mathcal{S}_{4\pi} = \mathcal{S}_{4\pi}^d + \mathcal{S}_{4\pi}^e + \mathcal{S}_{4\pi}^i$$

$$\begin{aligned}
\mathcal{S}_{4\pi}^d &= g_\pi^4 \mathcal{F}_\pi^4(t) [t^2] G_\pi(t) G_\pi(t)^* \\
\mathcal{S}_{4\pi}^e &= g_\pi^4 \mathcal{F}_\pi^4(u) [u^2] G_\pi(u) G_\pi(u)^* \\
\mathcal{S}_{4\pi}^i &= g_\pi^4 \mathcal{F}_\pi^2(t) \mathcal{F}_\pi^2(u) \left[ \frac{ut}{2} \right] \cdot \{G_\pi(t) G_\pi(u)^* + G_\pi(t)^* G_\pi(u)\}
\end{aligned}$$

$$\mathcal{S}_{2\pi 2\sigma} = \mathcal{S}_{2\pi 2\sigma}^d + \mathcal{S}_{2\pi 2\sigma}^e + \mathcal{S}_{2\pi 2\sigma}^i$$

$$\begin{aligned}
\mathcal{S}_{2\pi 2\sigma}^d &= 0 \\
\mathcal{S}_{2\pi 2\sigma}^e &= 0 \\
\mathcal{S}_{2\pi 2\sigma}^i &= g_\pi^2 g_\sigma^2 \left( \mathcal{F}_\sigma^2(t) \mathcal{F}_\pi^2(u) \left[ \frac{(4m_*^2 - t)u}{2} \right] \cdot \{G_\sigma(t) G_\pi(u)^* + G_\sigma(t)^* G_\pi(u)\} \right. \\
&\quad \left. + \mathcal{F}_\sigma^2(u) \mathcal{F}_\pi^2(t) \left[ \frac{(4m_*^2 - u)t}{2} \right] \cdot \{G_\sigma(u) G_\pi(t)^* + G_\sigma(u)^* G_\pi(t)\} \right)
\end{aligned}$$

$$\mathcal{S}_{2\pi 2\omega} = \mathcal{S}_{2\pi 2\omega}^d + \mathcal{S}_{2\pi 2\omega}^e + \mathcal{S}_{2\pi 2\omega}^i$$

$$\begin{aligned}
\mathcal{S}_{2\pi 2\omega}^d &= 0 \\
\mathcal{S}_{2\pi 2\omega}^e &= 0
\end{aligned}$$

$$\begin{aligned}
\mathcal{S}_{2\pi 2\omega}^i &= -g_\omega^2 g_\pi^2 \mathcal{F}_\omega^2(t) \mathcal{F}_\pi^2(u) \left( \left[ 4u(2m_*^2 - u) \right] \cdot \{G_{\omega T}(t)G_\pi^*(u) + G_{\omega T}^*(t)G_\pi(u)\} \right. \\
&\quad \left. + \left[ 8(4m_*^2 - s)p_{1\ominus}p_{4\ominus} - 4t(p_{1\ominus}^2 + p_{4\ominus}^2) + 2ut \right] \times \right. \\
&\quad \left. \times \{G_{\omega N}(t)G_\pi^*(u) + G_{\omega N}^*(t)G_\pi(u)\} \right) \\
&\quad - g_\omega^2 g_\pi^2 \mathcal{F}_\omega^2(u) \mathcal{F}_\pi^2(t) \left( \left[ 4t(2m_*^2 - t) \right] \cdot \{G_{\omega T}(u)G_\pi^*(t) + G_{\omega T}^*(u)G_\pi(t)\} \right. \\
&\quad \left. + \left[ 8(4m_*^2 - s)p_{1\oplus}p_{t\oplus} - 4u(p_{1\oplus}^2 + p_{3\oplus}^2) + 2ut \right] \times \right. \\
&\quad \left. \times \{G_{\omega N}(u)G_\pi^*(t) + G_{\omega N}^*(u)G_\pi(t)\} \right)
\end{aligned}$$

$$\mathcal{S}_{2\pi 1\sigma 1\omega} = \mathcal{S}_{2\pi 1\sigma 1\omega}^d + \mathcal{S}_{2\pi 1\sigma 1\omega}^e + \mathcal{S}_{2\pi 1\sigma 1\omega}^i$$

$$\mathcal{S}_{2\pi 1\sigma 1\omega}^d = 0$$

$$\mathcal{S}_{2\pi 1\sigma 1\omega}^e = 0$$

$$\begin{aligned}
\mathcal{S}_{2\pi 1\sigma 1\omega}^i &= -g_\sigma g_\omega g_\pi^2 \left( \mathcal{F}_\sigma(t) \mathcal{F}_\omega(t) \mathcal{F}_\pi^2(u) [8m_* u(p_{1\ominus} + p_{4\ominus})] \cdot \{G_\times(t)G_\pi^*(u) + G_\times^*(t)G_\pi(u)\} \right. \\
&\quad \left. \mathcal{F}_\sigma(u) \mathcal{F}_\omega(u) \mathcal{F}_\pi^2(t) [8m_* t(p_{1\oplus} + p_{3\oplus})] \cdot \{G_\times(u)G_\pi^*(t) + G_\times^*(u)G_\pi(t)\} \right)
\end{aligned}$$

## Acknowledgement

The authors would like to acknowledge the hospitality of GSI, Darmstadt, Germany and Subatech, Nantes, France where part of this work was performed.

## Figure captions

**Fig. 1:** N-N scattering through exchange of one dressed  $\pi$ ,  $\sigma$ ,  $\omega$  meson

**Fig. 2:** Fitting the experimental total elastic  $pp$  cross section: comparison of the performance of the various parameter sets. Experimental data points are indicated by the diamonds. The data set A, which is used for all calculations in this paper, corresponds to the full line.

**Fig. 3:** Fitting the experimental differential elastic cross section: (a) comes from a smoothed version of the compilation of existing experimental data for five values of the beam energy  $T_{\text{lab}} = 100, 300, 500, 700$  and  $900$  MeV. The dashed part on the left hand side of the figure corresponds to the range where Coulomb scattering is dominant and which was not taken into account for fitting. (b) Result of the fit for parameter set A and five values of the beam energy. (c) Differential cross section at saturation density and vanishing temperature, for five values of the beam energy.

**Fig. 4:** Total elastic  $p$ - $p$  cross section as a function of the beam energy at  $T=0$ , several densities. From top to bottom:  $n/n_{\text{sat}} = 0, 0.05, 0.1, 0.2, 0.5, 1., 2., 4.$

**Fig. 5:** Ratio of the value of the in-medium cross section to its value in the vacuum as a function of density  $n/n_{sat}$  (log. scale) for seven values of the temperature  $T=0, 40, 80, 120, 160, 200$  and  $240$  MeV.  $\sigma_{med}/\sigma_{free}$  is shown on (5a) for a beam energy  $T_{lab} = 100$  MeV and on (5b) for  $T_{lab} = 300$  MeV.

**Fig. 6:** (a) Ratio of the value of the in-medium cross section to its value in the vacuum as a function of temperature for five values of the density  $n/n_{sat}=0., 0.1, 1., 2.$  and  $4.$  and for two values of the beam energy  $T_{lab}=100$  MeV (full line) and  $T_{lab}=300$  MeV (dashed line). (b), The effective mass of the nucleon as a function of temperature is shown for comparison.

**Fig. 7:** Ratio of the value of the in-medium cross section to its free value: Contour plot in the density-temperature  $\log_{10}(n/n_{sat})$  vs.  $T$  plane, for three values of the energy of the incident particles  $T_{lab}=100, 300$  and  $500$  MeV.

**Fig. 8:** Differential elastic  $p$ - $p$  cross section at  $T = 0$  as a function of the scattering angle, for a value of the beam energy  $T_{lab} = 800$  MeV, and several densities:  $n/n_{sat} = 0, 0.05, 0.2, 0.5, 1., 2., 4.$

**Fig. 9:** Ratio of the “effective masses” (as defined in Eq. 27) to their value in the vacuum, and mixing parameter (Eq. 29), as a function of momentum transfer at  $T=0, n/n_{sat} = 0.1$ . There is a critical value of the momentum transfer  $q = 2p_F$ . Also shown are the values of the dynamical masses obtained by solving the dispersion relation at zero 3-momentum  $k = (\omega_i^{pl}, \vec{0})$ :  $\mu_i^{dyn} = \omega_i^{pl}, D(k) = 0$ .

**Fig. 10:** Comparison of experimental constraints on the reduction factor on the in-medium cross section from BUU and AMD, Brueckner calculations, and our model. The BUU calculation is represented by the calculation of Klakow and is indicated by two arrows for densities  $n/n_{sat}=1.$  and  $0.5$ . The AMD calculation is represented by the results of a simulation by Tanaka *et al.* of  $p+{}^9\text{Be}$  (diamonds) and  $p+{}^{40}\text{Ca}$  (triangles) collisions, thought to probe densities  $n/n_{sat} \simeq 0.1$  and  $1.$  respectively. Theoretical results calculating the medium effects in the Brueckner approach are taken from the paper of Li and Machleidt at densities  $n/n_{sat} = 0.5$  (dotted line) and  $1.$  (full line) and vanishing temperature. The results of this work are displayed for two values of the temperature  $T = 0$  (thin lines) and  $T = 50$  MeV (thick lines) and two values of the density  $n/n_{sat} = 0.1$  (dashed lines) and  $n/n_{sat} = 1.$  (dash-dotted line).

**Fig. 11:** The  $\omega$ - $q$  plane, particle/hole damping region and zero sound branches. The zero-sound branches are calculated for  $g_\sigma = 3.8, g_\omega = 9.3$  without form factors. For a fixed value of the beam energy, scattering angle and quadri-momentum transfer, and by varying the relative velocity existing between the rest system of the fluid and the center of mass of the collision, the point of coordinates  $(\omega$ - $q)$  describes a line which may twice cross the zero sound branches.

## References

- [1] J. Diaz Alonso, A. Perez and H. Sivak, Nucl. Phys. **A205** (1989) 695.
- [2] E. Gallego, J. Diaz Alonso and A. Pérez, Nucl. Phys. **A578** (1994) 542; J. Diaz Alonso, E. Gallego and A. Perez, Phys. Rev. Lett. **73** (1994) 2536.
- [3] J. Cugnon, T. Mizutani and J. Vandermeulen, Nucl. Phys. **A352** (1981) 505.
- [4] D. Klakow, G. Welke and W. Bauer, Phys. Rev. **C48** (1993) 1982.

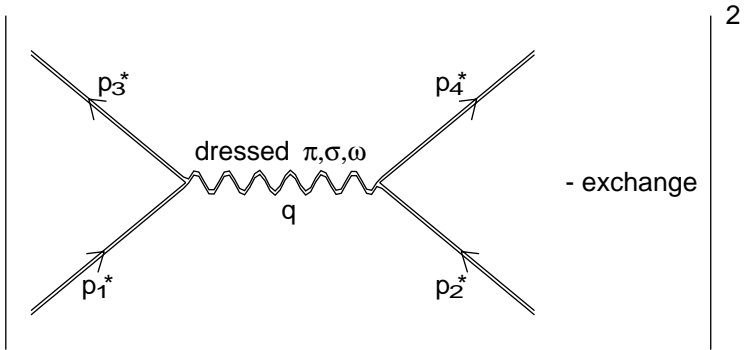
- [5] G.D. Westfall *et al.*, Phys. Rev. Lett. **71** (1993) 1986.
- [6] V. de la Mota, F. Sebille, M. Farine, B. Remaud and P. Schuck, Phys. Rev. **C46** (1992) 677.
- [7] B.A. Li, Phys. Rev. **C48** (1993) 2415.
- [8] T. Alm, G. Röpke, W. Bauer, F. Daffin and M. Schmidt, Nucl. Phys. **A587** (1995) 815.
- [9] D.T. Khoa, N. Ohtsuka, M.A. Matin, A. Faessler, S.W. Huang, E. Lehman and R. Puri, Nucl. Phys. **A 548** (1992) 102.
- [10] E.I. Tanaka, A. Ono, H. Horiuchi, T. Maruyama and E. Engel, Phys. Rev. **C52** (1995) 316.
- [11] A. Faessler, Nucl. Phys. **A495** (1989) 103c; A. Bohnet, N. Ohtsuka, J. Aichelin, R. Linden and A. Faessler, Nucl Phys. **A494** (1989) 349.
- [12] C. Fuchs, L. Sehn and H.H. Wolter, Nucl. Phys. **A601** (1996) 505.
- [13] B. Ter Haar and R. Malfliet, Phys. Rev. **C36** (1987) 1611.
- [14] J. Cugnon, A. Lejeune and P. Grangé, Phys. Rev. **C35** (1987) 861.
- [15] G.Q. Li and R. Machleidt, Phys. Rev. **C48** (1993) 1702.
- [16] G.Q. Li, R. Machleidt, *Phys. Rev.* **C49** (1994) 566.
- [17] T. Alm, G. Röpke and M. Schmidt, *Phys. Rev.* **C50** (1994) 31.
- [18] M. Schönhofen, M. Cubero, B.L. Friman, W. Nörenberg and Gy. Wolf, Nucl. Phys. **A572** (1994) 112.
- [19] Mao Guangjun, Li Zhuoxia, Zhuo Yizhong, Han Yinlu, Yu Ziqiang and M. Sano, Z. Phys. **A347** (1994) 173.
- [20] R. Machleidt. “The Meson Theory of Nuclear Forces and Nuclear Structure.” Adv. in Nucl. Phys. Vol.**19**; J.W. Negele and E. Vogt Edts. (Plenum, New York, 1989.)
- [21] E. Oset, H. Toki and W. Weise, Phys. Rep. **83** (1982) 281.
- [22] T. Herbert, K. Wehrberger and F. Beck, Nucl. Phys. **A541** (1992) 699.
- [23] P. Arve and J. Helgesson, Nucl. Phys. **A572** (1994) 600; J. Helgesson and J. Randrup, Ann. Phys. **244** (1995) 12.
- [24] B.D. Serot, J.D. Walecka, “The Relativistic Nuclear Many-Body Problem”, Adv. in Nucl. Phys., **16**, J.W. Negele and E. Vogt Edts. ( Plenum, New York, 1986).
- [25] S.A. Chin, Ann. Phys. **108** (1977) 301.
- [26] J. Diaz Alonso, Annals of Phys. **160** (1985) 1.
- [27] T. Matsui and B.D. Serot, Ann. Phys. (N.Y.) **144** (1982) 107.
- [28] R. Hakim, Riv. Nuovo Cimento **1** (1978) 1.
- [29] J. Diaz Alonso and A. Pérez Canyellas, Nucl. Phys. **A526** (1991) 623.
- [30] K. Lim and C.J. Horowitz, Nucl. Phys. **A501** (1989) 729.
- [31] K. Saito, T. Maruyama, Phys. Rev. **C40**, (1989), 407.
- [32] J. Diaz Alonso, B. Friman, P.A. Henning, “Normal Modes in Nuclear Matter at Finite Temperature”. Unpublished preprint G.S.I. Darmstadt (1992). Some results of this last reference have been published in P.A. Henning, Phys. Rep. **253** (1995), 235.

- [33] J. Diaz Alonso, Phys. Rev. **D31** (1985), 1315.
- [34] B. Friman and P. Henning, Phys. Lett. **B206** (1988) 579.
- [35] S. Weinberg, "The Quantum Theory of Fields" (Cambridge Univ. Press, 1995).
- [36] G. Krein, M. Nielsen, R.D. Puff and L. Willets, Phys. Rev. **C47** (1993) 2485.
- [37] M.P. Allendes and B.D. Serot, Phys. Rev. **C45** (1992) 2975; B.D. Serot and H.B. Tang, Phys. Rev. **C51** (1991) 969.
- [38] R.A. Arndt, I.I. Strakovskii and R.L. Workman, Phys. Rev. **C52** (1995) 2246; R.A. Arndt, I.I. Strakovskii, R.L. Workman and M. Pavan,  $\pi$ -N Newslett. **8** (1993) 37.
- [39] R.M. Barnett *et al.* (Particle Data Group), Phys. Rev. **D54** (1996) 1.
- [40] M. Svec, Phys. Rev. **D53** (1996) 2343; N.A. Törnqvist and M. Roos, Phys. Rev. Lett. **76** (1996) 1575.
- [41] J. Hamilton and G.C. Oades, Nucl. Phys. **A424** (1984) 447.
- [42] N. Kaiser, U. Vogl, W. Weise and U.-G. Meissner, Nucl. Phys. **A484** (1988) 593.
- [43] K. Saito and A.W. Thomas, Phys. Lett. **B327** (1994) 9.
- [44] V. Stoks, J.J. de Swart, Phys. Rev. **C47**, (1993), 761;  
V.G.J. Stoks, R.A.M. Klomp, M.C.M. Rentmeester and J.J. de Swart, Phys. Rev. **C48** (1993) 792  
NN-Online Database, available on the Nijmegen WWW pages (URL: <http://nn-online.sci.kun.nl/>)
- [45] R.A. Arndt, I.I. Strakovskii and R.L. Workman, Phys. Rev. **C50**, 2731 (1994).  
Scattering Analysis Interactive Dial-in (SAID) program available *via* telnet, connecting to vtinte.phys.vt.edu with user/password: physics/quantum.
- [46] J. Cugnon and M.C. Lemaire, Nucl. Phys. **A489** (1988) 781.
- [47] K. Chen, Z. Fraenkel, G. Friedlander, J.R. Grover, J.M. Miller and Y. Shimamoto, Phys. Rev. **166** (1968) 949.
- [48] R. Machleidt, K. Holinde and Ch. Elster, Phys. Rep. **149** (1987) 1.
- [49] R. Machleidt, F. Sammarruca, and Y. Song, Phys. Rev. **C53** (1996) 1483.
- [50] V.G.J. Stoks, R.A.M. Klomp, C.P.F. Terheggen and J.J. de Swart, Phys. Rev. **C49** (1994) 2950.
- [51] R.B. Wiringa, V.G.J. Stoks and R. Schiavilla, Phys. Rev. **C51** (1995) 83.
- [52] A.D. Jackson and T. Wettig, Phys. Rep. **237** (1994) 325.
- [53] E. Alvarez, Phys. Lett. **B110** (1982) 315.
- [54] E.I. Tanaka, H. Horiuchi and A. Ono, "Determination of *in-medium* nucleon-nucleon cross section from the data of proton-induced reaction cross section" preprint Kyoto U. KUNS 1364 (1996)
- [55] E.I. Tanaka, A. Ono, H. Horiuchi, T. Maruyama and A. Engel, Phys. Rev. **C52** (1995) 316.
- [56] C. Ordoñez, L. Ray and U. van Kolck, Phys. Rev. Lett. **72** (1994) 1982.
- [57] R.J. Furnstahl, B.D. Serot and H.B. Tang, Nucl. Phys. **A615** (1997) 441.



- [58] V.G.J. Stoks and Th.A. Rijken, Nucl. Phys. **A613** (1997) 311.
- [59] S. Huber and J. Aichelin, Nucl. Phys. **A573** (1994) 587.
- [60] G.F. Bertsch, G.E. Brown, V. Koch and B.A. Li, Nucl. Phys. **A490** (1988) 745.
- [61] Guangjun Mao, Zhuxia Li, Yizhang Zhuo and Enguang Zhao, Phys. Rev. **C55** (1997) 792.
- [62] K. Wehrberger, C. Bedau and F. Beck, Nucl. Phys. **A504** (1989) 797.

Fig. 1





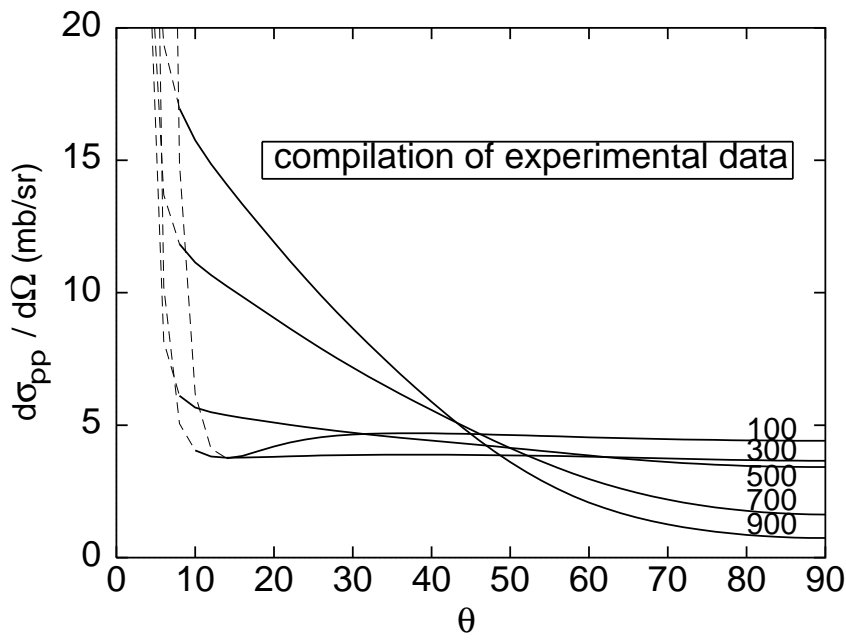


Fig. 3a

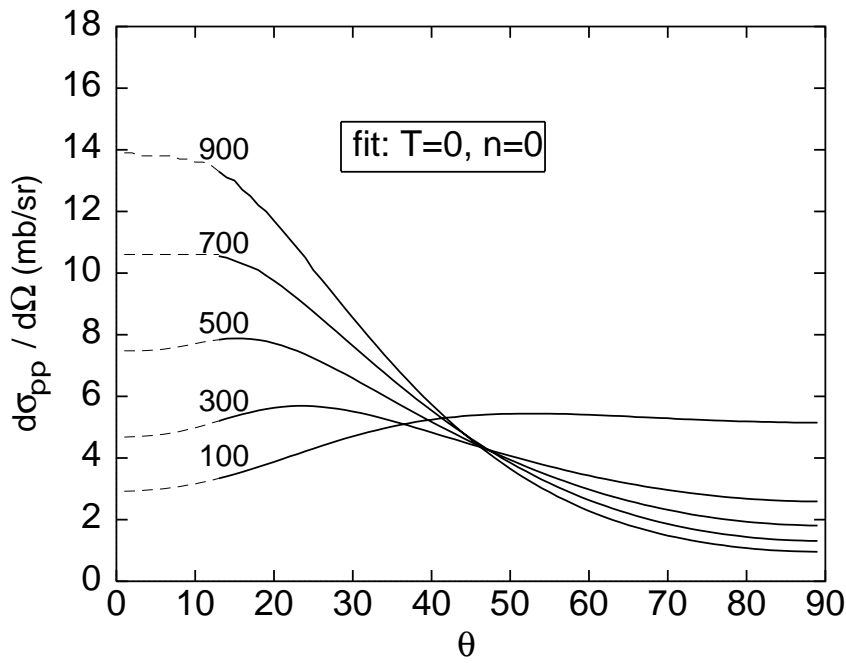


Fig. 3b

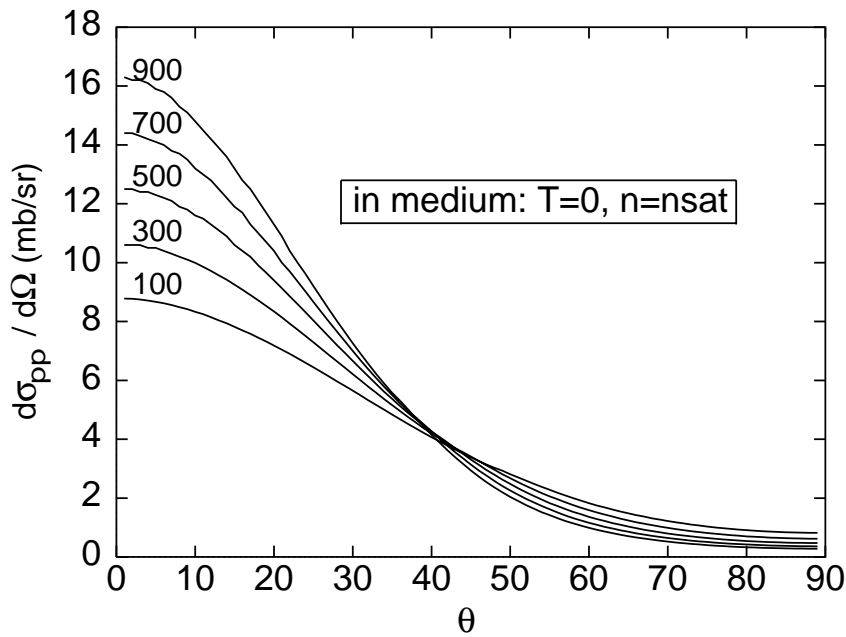
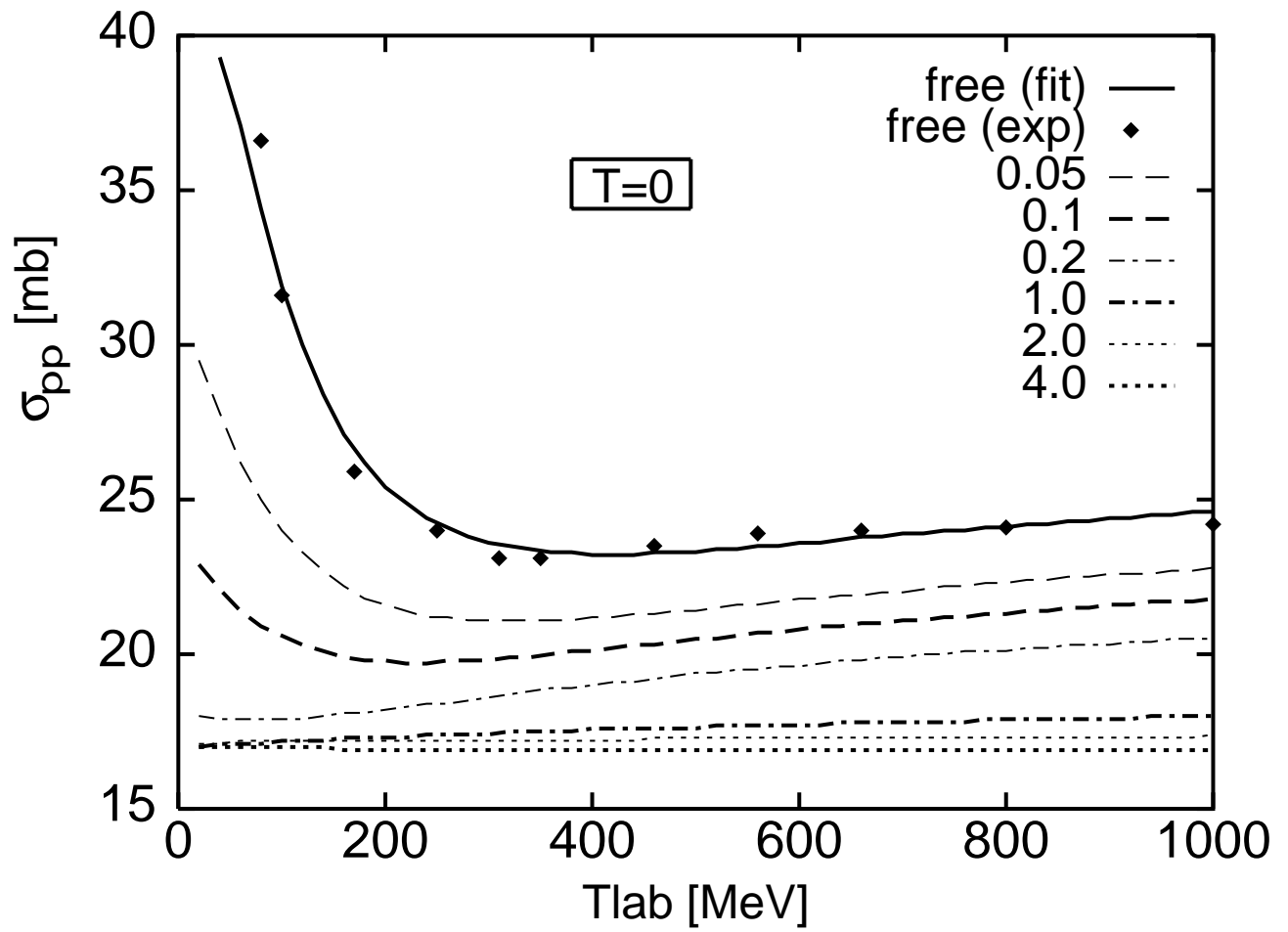
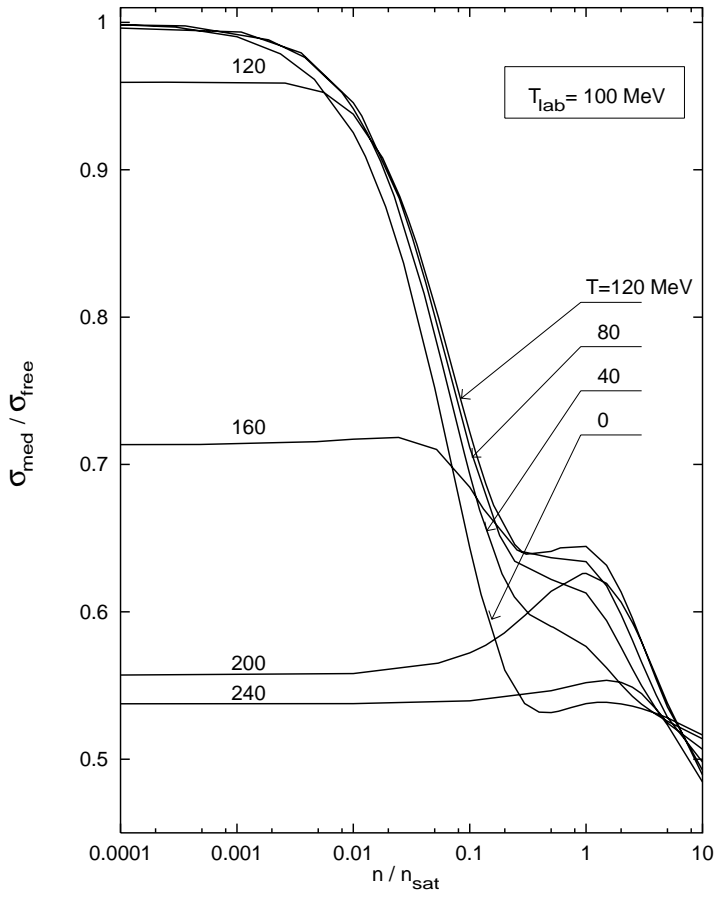


Fig. 3c

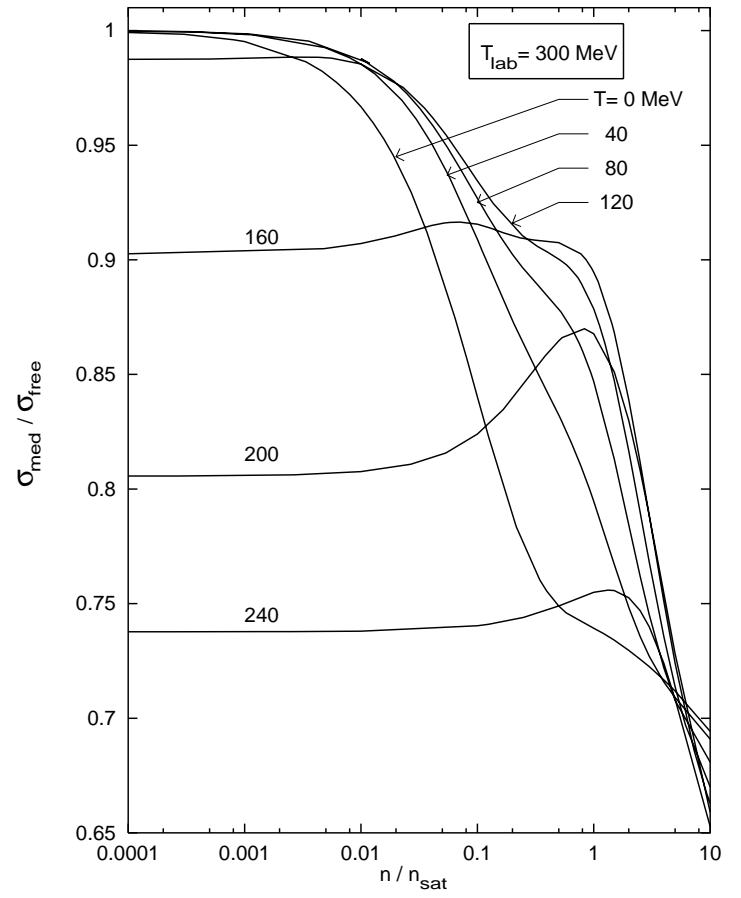
Fig. 4

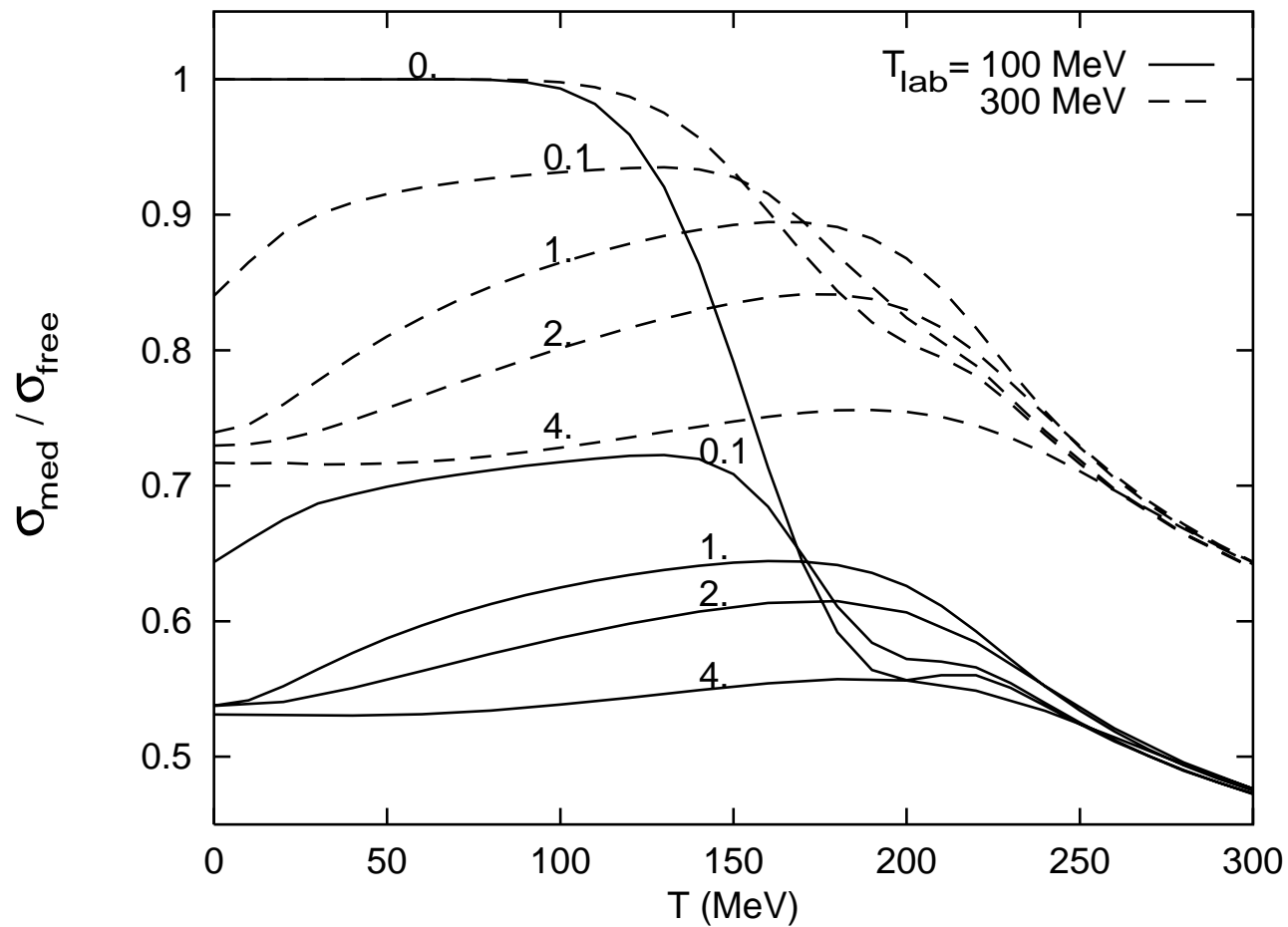
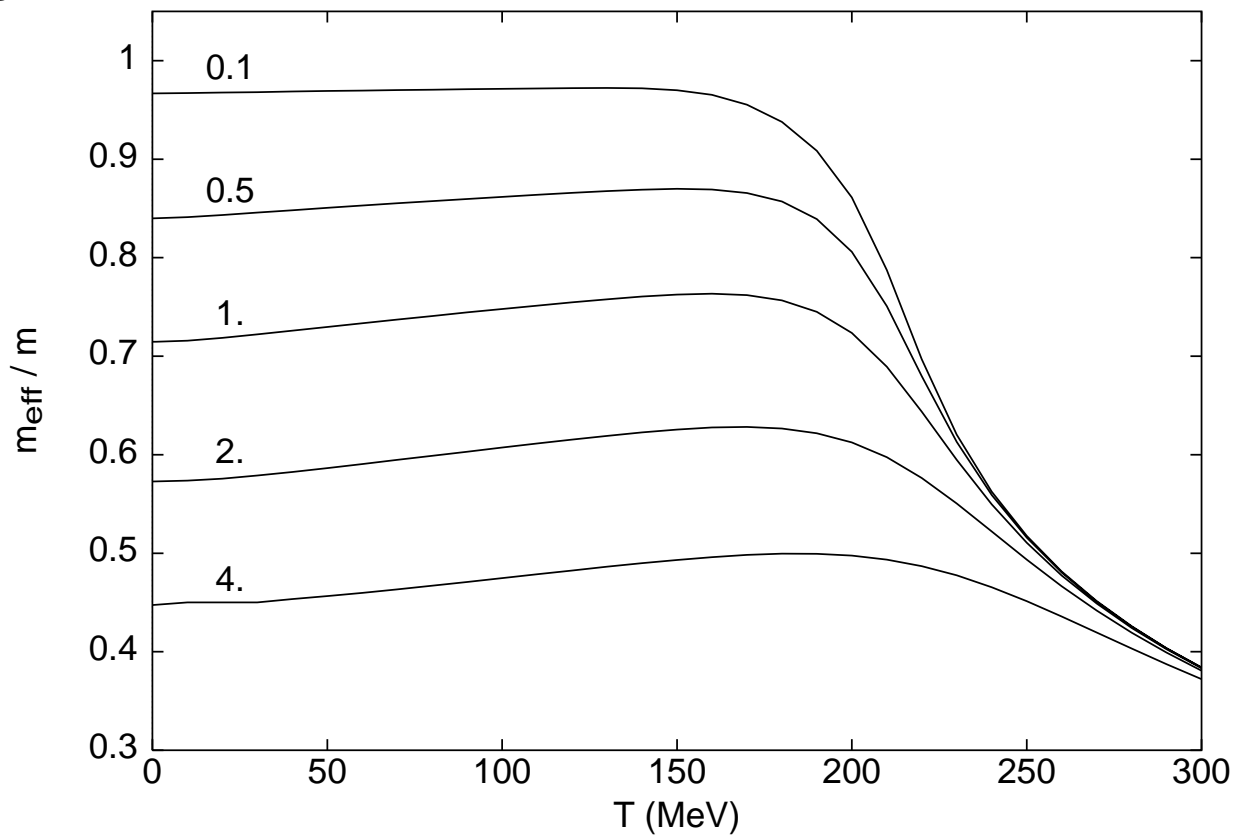


**Fig. 5a**



**Fig. 5b**



**Fig. 6a****Fig. 6b**

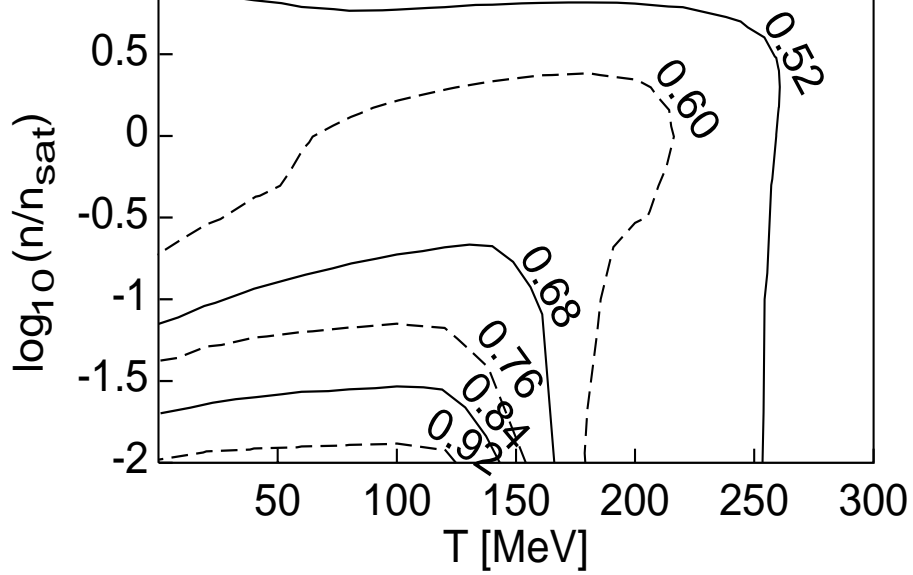


Fig. 7a

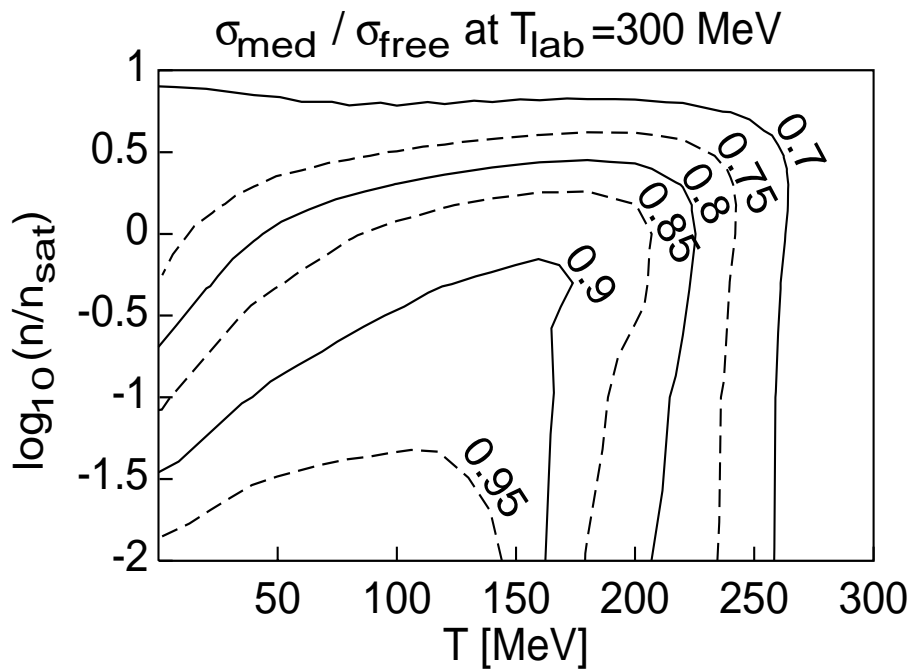


Fig. 7b

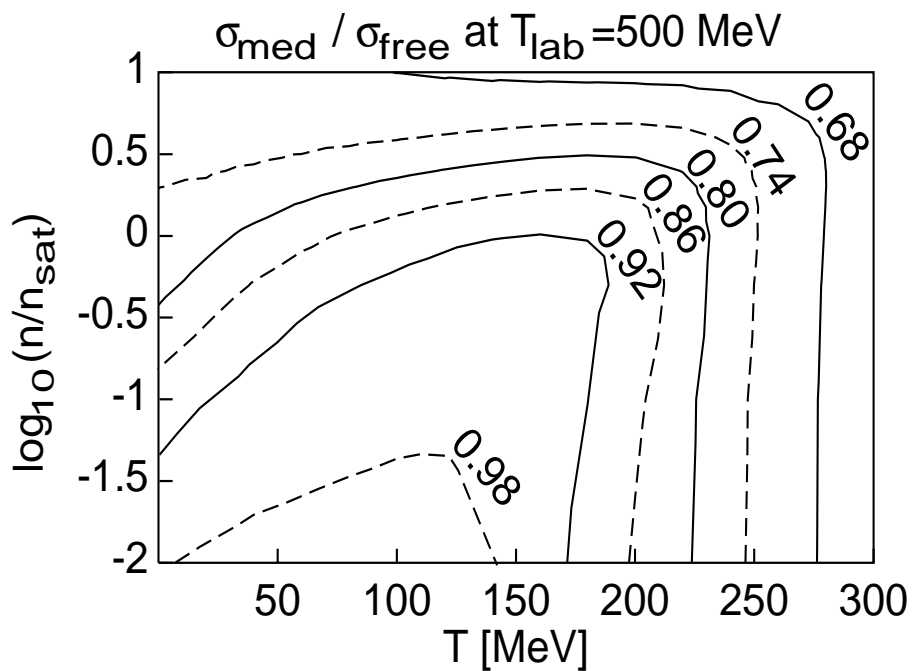


Fig. 7c



**Fig. 8**

Differential elastic pp cross section at  $T_{\text{lab}}=800$  MeV  
several densities (in units  $n_{\text{sat}}$ )

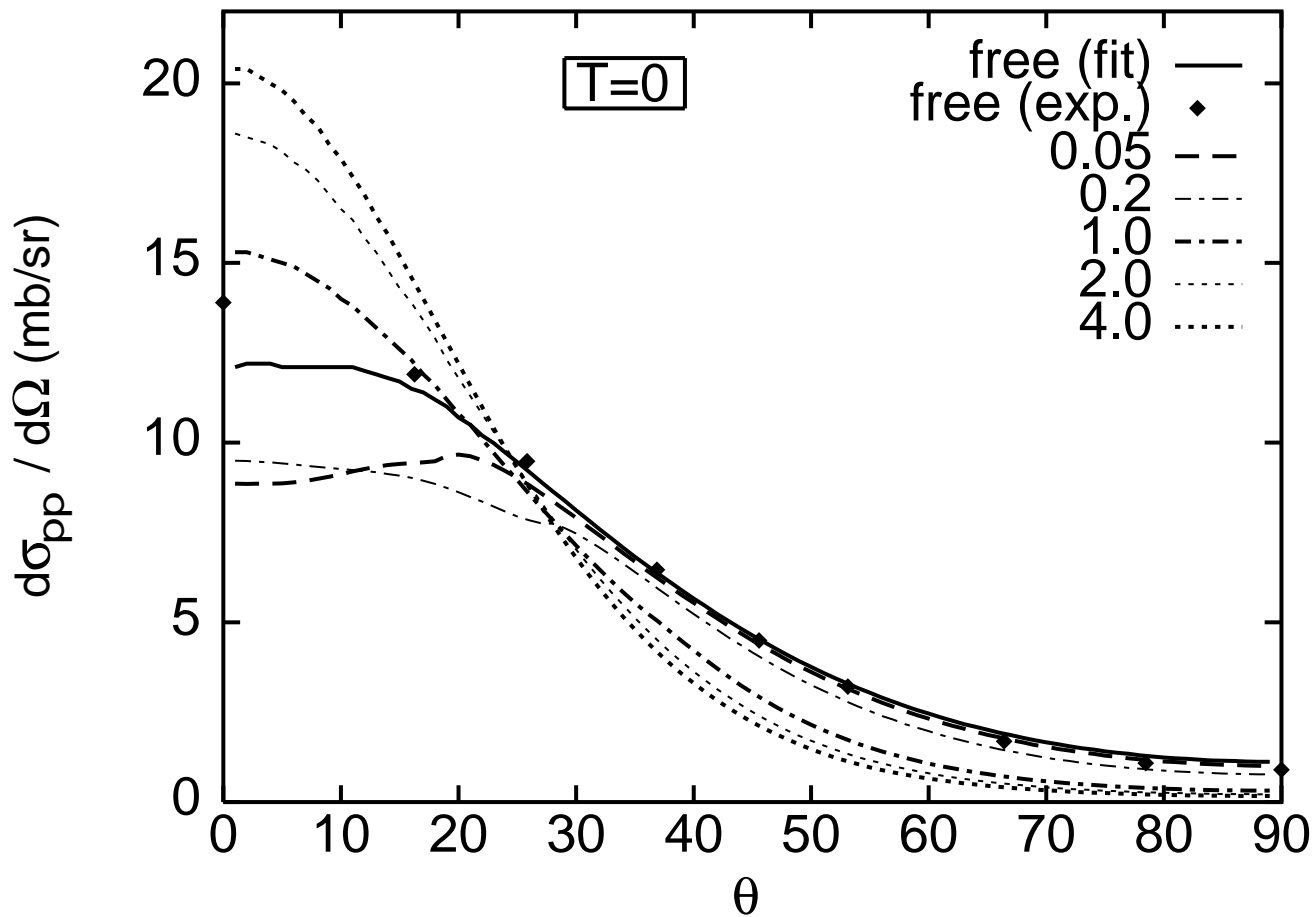
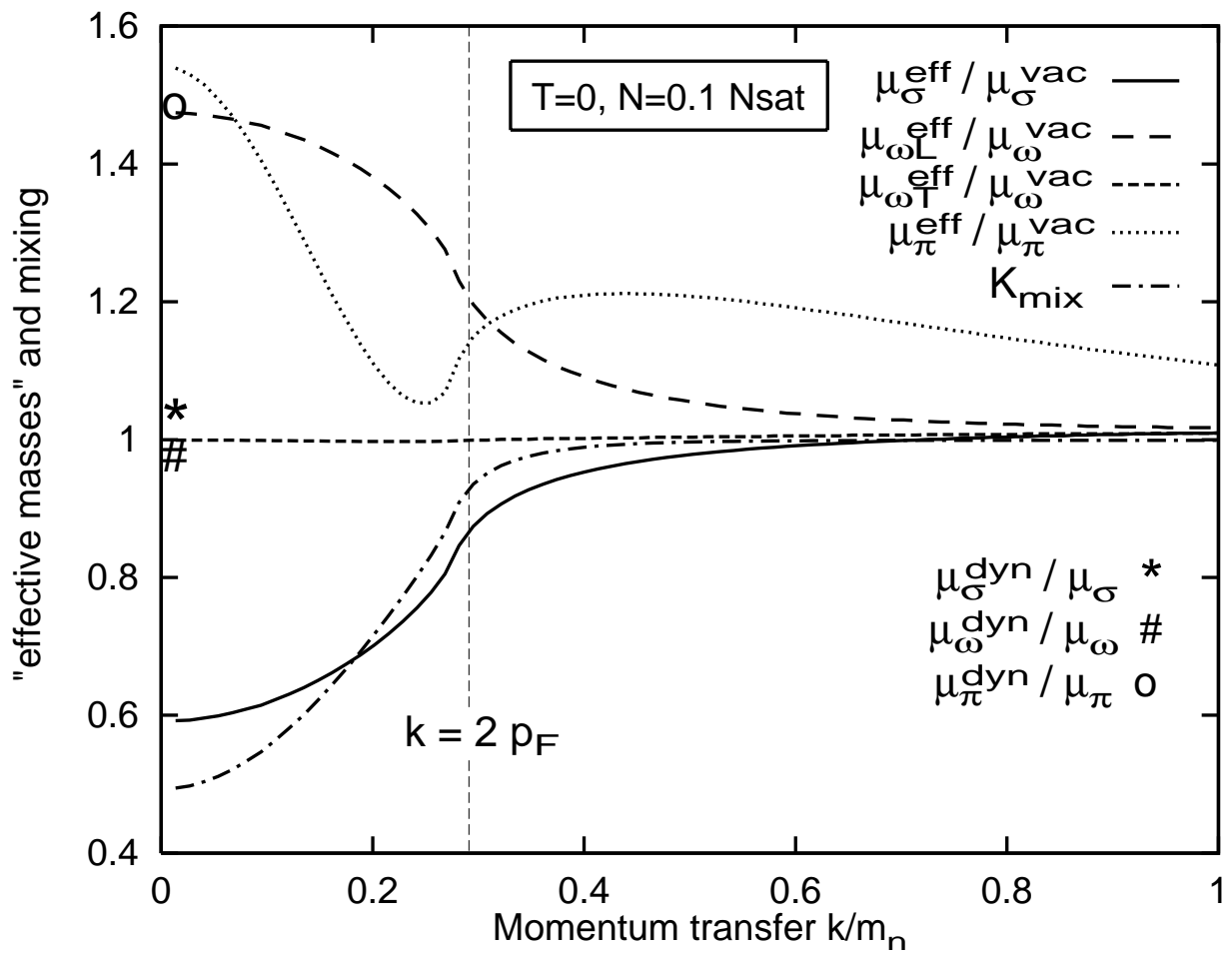
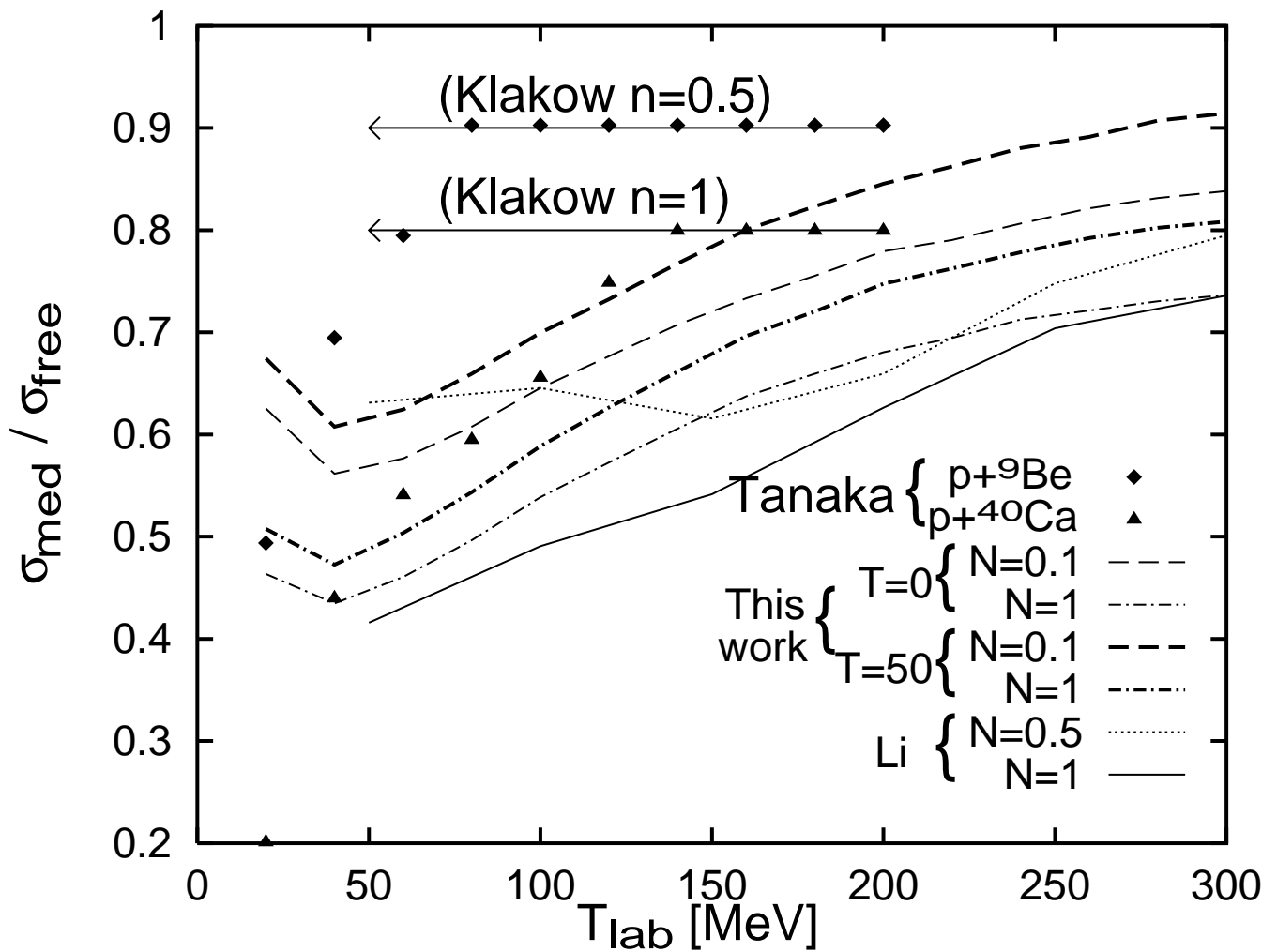


Fig. 9



**Fig. 10**



**Fig. 11**

